Dissecting the genetic complexity of myalgic encephalomyelitis/chronic fatigue syndrome via deep learning-powered genome analysis

Sai Zhang[1,2,3,*,†], Fereshteh Jahanbani[1,*], Varuna Chander[1,*], Martin Kjellberg[1,*], Menghui Liu[2], Katherine A. Glass[4], David S. Iu[4], Faraz Ahmed[5], Han Li[6], Rajan Douglas Maynard[1], Tristan Chou[1], Johnathan Cooper-Knock[7], Martin Jinye Zhang[8], Durga Thota[1], Michael Zeineh[9], Jennifer K. Grenier[5], Andrew Grimson[4], Maureen R. Hanson[4], Michael P. Snyder[1,†]

[1]Department of Genetics, Center for Genomics and Personalized Medicine, Stanford University School of Medicine, Stanford, CA, USA
[2]Department of Epidemiology, University of Florida, Gainesville, FL, USA
[3]Department of Biostatistics & Biomedical Engineering, Genetics Institute, McKnight Brain Institute, University of Florida, Gainesville, FL, USA
[4]Department of Molecular Biology and Genetics, Cornell University, Ithaca, NY, USA
[5]Genomics Facility, Biotechnology Resource Center, Cornell University, Ithaca, NY, USA
[6]School of Mathematical Sciences and LPMC, Nankai University, Tianjin, China
[7]Sheffield Institute for Translational Neuroscience, University of Sheffield, Sheffield, UK
[8]Ray and Stephanie Lane Computational Biology Department, Carnegie Mellon University, Pittsburgh, PA, USA
[9]Department of Radiology, Stanford University School of Medicine, Stanford, CA, USA

*These authors contributed equally: Sai Zhang, Fereshteh Jahaniani, Varuna Chander, and Martin Kjellberg
[†]Correspondence: sai.zhang@ufl.edu; mpsnyder@stanford.edu

Abstract

Myalgic encephalomyelitis/chronic fatigue syndrome (ME/CFS) is a complex, heterogeneous, and systemic disease defined by a suite of symptoms, including unexplained persistent fatigue, post-exertional malaise (PEM), cognitive impairment, myalgia, orthostatic intolerance, and unrefreshing sleep. The disease mechanism of ME/CFS is unknown, with no effective curative treatments. In this study, we present a multi-site ME/CFS whole-genome analysis, which is powered by a novel deep learning framework, HEAL2. We show that HEAL2 not only has predictive value for ME/CFS based on personal rare variants, but also links genetic risk to various ME/CFS-associated symptoms. Model interpretation of HEAL2 identifies 115 ME/CFS-risk genes that exhibit significant intolerance to loss-of-function (LoF) mutations. Transcriptome and network analyses highlight the functional importance of these genes across a wide range of tissues and cell types, including the central nervous system (CNS) and immune cells. Patient-derived multi-omics data implicate reduced expression of ME/CFS risk genes within ME/CFS patients, including in the plasma proteome, and the transcriptomes of B and T cells, especially cytotoxic CD4 T cells, supporting their disease relevance. Pan-phenotype analysis of ME/CFS genes further reveals the genetic correlation between ME/CFS and other complex diseases and traits, including depression and long COVID-19. Overall, HEAL2 provides a candidate genetic-based diagnostic tool for ME/CFS, and our findings contribute to a comprehensive understanding of the genetic, molecular, and cellular basis of ME/CFS, yielding novel insights into therapeutic targets. Our deep learning model also offers a potent, broadly applicable framework for parallel rare variant analysis and genetic prediction for other complex diseases and traits.

Introduction

Myalgic encephalomyelitis/chronic fatigue syndrome (ME/CFS) is a complex and debilitating multisystem disorder that affects millions of people, with an estimated 65 million individuals living with the condition worldwide prior to 2020[1]. It has a complex and heterogeneous manifestation that presents with a broad spectrum of debilitating symptoms. ME/CFS occurs with other debilitating symptoms, such as post-exertional malaise, unrefreshing sleep, and cognitive dysfunction[2]. The impact of this condition is far-reaching, with one in four patients becoming housebound or bedbound, and many of the most severely affected individuals requiring feeding tubes[3]. As a significant diagnostic challenge, ME/CFS is often misdiagnosed or undiagnosed due to the lack of a definitive biomarker, with 90% of the individuals frequently undergoing a prolonged diagnostic odyssey after years of medical consultation[4].

ME/CFS can affect individuals of all ages, races, ethnicities, and socioeconomic backgrounds, making it a universal threat[5]. Unfortunately, there are no FDA-approved treatments for the disease, and current management strategies focus primarily on symptom relief. This lack of specific treatments highlights the urgent need for more robust research into the disease's etiology and pathogenesis.

Despite its significant impact, ME/CFS remains poorly understood, with its underlying mechanisms still largely unknown. A combination of genetic, infectious, and environmental factors may contribute to disease onset and progression. A majority of individuals with ME/CFS report a preceding viral-like infection and clustered outbreaks have occurred in the past[6]. However, not everyone who suffers a viral infection develops ME/CFS nor can all cases be traced to a symptomatic viral illness; therefore understanding the genetic basis of susceptibility to ME/CFS is critical, as it could not only illuminate the underlying mechanisms of the disease, but also open the door for novel diagnostics and therapeutic interventions. Recent advances in genomics and the growing recognition that ME/CFS exhibits genetic risk factors[7] present new opportunities for research. Previous genetic studies[8,9] have been limited by small sample sizes and inconsistent results, highlighting the need for large-scale, well-characterized patient cohorts, and advanced methodology to uncover meaningful genetic insights.

We provide a large whole-genome analysis of ME/CFS, powered by the novel deep learning framework HEAL2. Based on rare coding variants, HEAL2 predicted ME/CFS risk for individuals across multiple cohorts. This approach further identified 115 risk genes associated with ME/CFS exhibiting critical functional roles across various tissues and cell types, including the central nervous system (CNS) and immune cells. Multi-omics data from ME/CFS patients validated the relevance of these findings, showing reduced expression of these genes in affected individuals. Finally, our pan-phenotype analysis uncovered a genetic correlation between ME/CFS and other conditions, such as depression and long COVID-19. Our study not only contributes to a deeper understanding of the genetic basis of ME/CFS, but also provides a powerful, generic framework for conducting rare variant analysis in other complex diseases. By deriving a genetic risk score and identifying some genetic risk factors associated with ME/CFS, this research holds the future potential to catalyze the development of precision diagnosis and effective therapies, providing much-needed hope for the millions of people living with this life-altering disease.

Results

Whole-genome sequencing of multiple ME/CFS cohorts

We conducted whole-genome sequencing (WGS) on the same platform for *N* = 1,075 individuals (*N* = 464 ME/CFS patients, *N* = 611 negative controls) from three ME/CFS cohorts (**Fig. 1A**; **Methods**): (1) a Stanford cohort that we assembled (*N* = 208 cases, *N* = 534 controls; see methods), (2) a UK CureME cohort (*N* = 190 cases, *N* = 30 controls), and (3) a Cornell cohort (*N* = 66 cases, *N* = 47 controls). To increase the sample size of ME/CFS cases, we combined the Stanford and CureME cohorts into the discovery cohort and used the Cornell cohort as an independent testing cohort. After read alignment, variant calling, stringent quality controls (QCs), and ancestry analysis (**Methods**), we obtained the analysis-ready discovery cohort (*N* = 247 cases, *N* = 192 controls) and testing cohort (*N* = 36 cases, *N* = 21 controls). In particular, non-European and genetically-related individuals were excluded to control sampling bias (**Methods**).

We performed variant annotation for all genetic variants, including the single nucleotide variants (SNVs) and small insertions and deletions (indels), within the analysis-ready cohorts (**Fig. 1A**; **Methods**). In this study, we mainly focused on the coding variants including the loss-of-function (LoF) variants and missense (nonsynonymous) variants, wherein missense variants were further annotated using 38 functional scores (**Methods**). We have focused on rare variants, which are more likely to be functionally significant[10], and are less likely to be confounded by linkage disequilibrium (LD). Given the moderate sample size of our cohorts, we used gnomAD[11] (version 4.1, Non-Finnish European [NFE]) to estimate allele frequencies (AFs), and retained 99,958 rare coding variants (NFE AF < 1%) for downstream machine learning analysis (**Fig. 1A**).

HEAL2 predicts ME/CFS risk from personal rare variants

To model the rare-variant genetic architecture of ME/CFS, we developed HEAL2, a graph neural network (GNN)-based framework that predicts ME/CFS risk from personal rare coding variants (**Fig. 1A**; **Methods**). HEAL2 extends our previous method HEAL[12] in three aspects: (1) HEAL2 incorporates more comprehensive variant categories and functional scores; (2) HEAL2 employs an attention mechanism to improve model interpretation; (3) HEAL2 contains a non-linear GNN component based on the protein-protein interaction (PPI) network to capture the epistasis underpinning phenotypes, while HEAL is a linear model. Briefly speaking, for each individual HEAL2 first computes gene-level burden scores based on a variety of variant categories and functional scores using max and sum pooling (**Fig. 1A**; **Methods**). Next, HEAL2 conducts message passing of gene embeddings based on known PPIs. A sparse autoencoder (SAE)-based attention operation is then placed over gene embeddings after GNN to facilitate gene prioritization. Gene embeddings are pooled using attentions to construct a network embedding, which is used to compute the final ME/CFS risk score.

We first assessed the capacity of HEAL2 in modeling nonlinear genotype-phenotype (G2P) mapping using simulations. Based on a simulated nonlinear G2P dataset, we found that HEAL2 accurately predicted the disease from rare variants (area under the receiver operating characteristic curve [AUROC] : 0.891 [mean] ± 0.002 [95% CI]; area under the precision-recall curve [AUPRC]: 0.876 ± 0.001; **Supplementary Fig. 1A** and **1B**), significantly outperforming HEAL in comparison (AUROC: 0.598 ± 0.004; AUPRC: 0.548 ± 0.005; **Supplementary Fig. 1A**

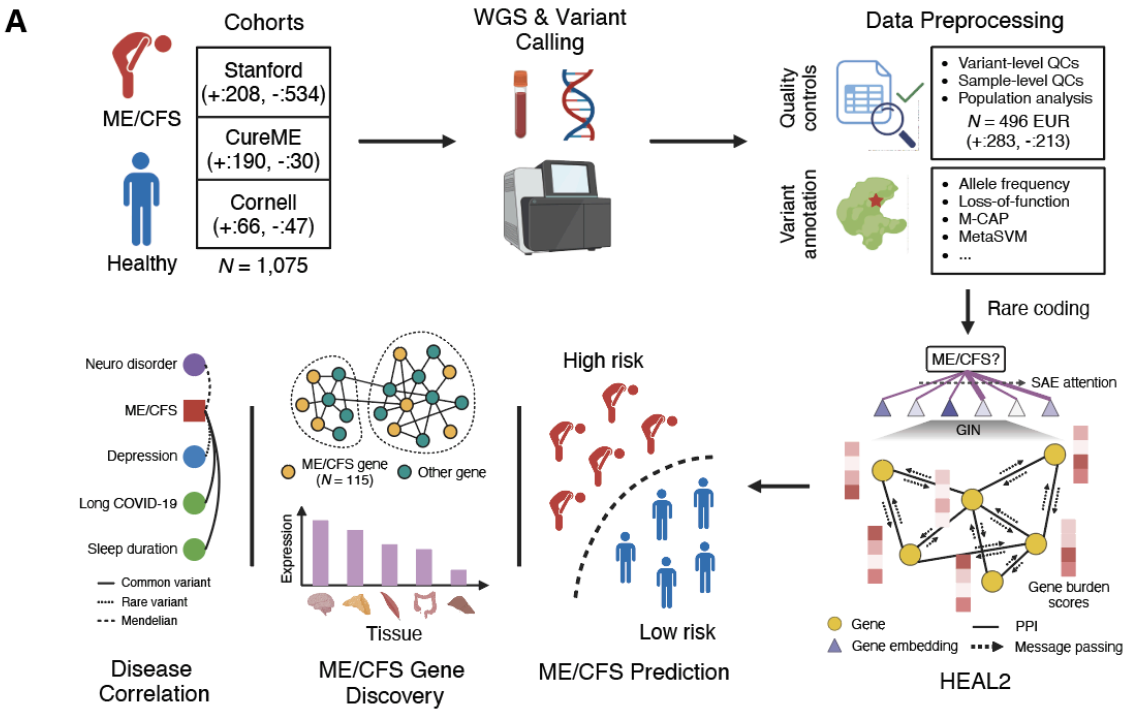
A
Cohorts
ME/CFS
Healthy
Stanford (+:208, -:534)
CureME (+:190, -:30)
Cornell (+:66, -:47)
N = 1,075
WGS & Variant Calling
Data Preprocessing
Quality controls
Variant-level QCs
Sample-level QCs
Population analysis
N = 496 EUR (+:283, -:213)
Variant annotation
Allele frequency
Loss-of-function
M-CAP
MetaSVM
...
Rare coding
ME/CFS?
SAE attention
GIN
Gene burden scores
Gene
Gene embedding
PPI
Message passing
HEAL2
High risk
Low risk
ME/CFS Prediction
ME/CFS gene (N = 115)
Other gene
Expression
Tissue
ME/CFS Gene Discovery
Neuro disorder
ME/CFS
Depression
Long COVID-19
Sleep duration
Common variant
Rare variant
Mendelian
Disease Correlation

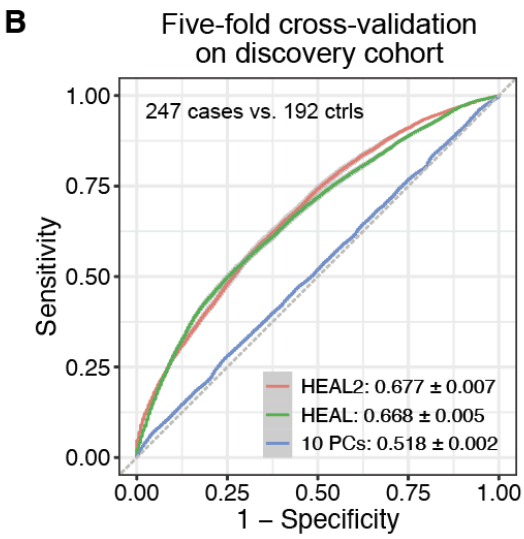
B
Five-fold cross-validation on discovery cohort
247 cases vs. 192 ctrls
Sensitivity
1 – Specificity
HEAL2: 0.677 ± 0.007
HEAL: 0.668 ± 0.005
10 PCs: 0.518 ± 0.002

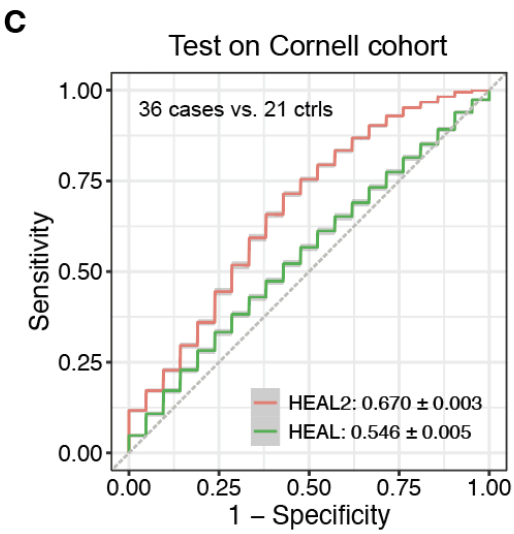
C
Test on Cornell cohort
36 cases vs. 21 ctrls
Sensitivity
1 – Specificity
HEAL2: 0.670 ± 0.003
HEAL: 0.546 ± 0.005

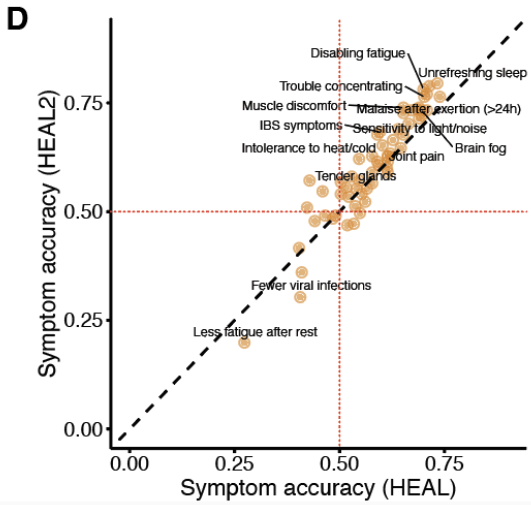
D
Disabling fatigue
Unrefreshing sleep
Trouble concentrating
Muscle discomfort
Malaise after exertion (>24h)
IBS symptoms
Sensitivity to light/noise
Intolerance to heat/cold
Brain fog
Joint pain
Tender glands
Fewer viral infections
Less fatigue after rest
Symptom accuracy (HEAL2)
Symptom accuracy (HEAL)

Figure 1. HEAL2 study design and prediction performance. (A) Schematic of our study design and HEAL2 model architecture. +, ME/CFS case; -, negative control; WGS, whole-genome sequencing; QCs, quality controls; EUR, European; GIN, graph isomorphism network; SAE, sparse autoencoder; PPI, protein-protein interaction. (B) Prediction performance of five-fold cross-validation (100 repeats) on the discovery cohort. The curve and shaded area represent the AUROC mean and 95% confidence interval (CI), respectively. AUROC, area under the receiver operating characteristic curve; PC, principal component. (C) Prediction performance of testing (500 repeats) on the independent Cornell cohort. The curve and shaded area represent the AUROC mean and 95% CI, respectively. (D) Correlation between genetic risk scores and patient symptoms. We examined the correlation by computing the accuracy of HEAL or HEAL2 on predicting different patient symptoms. The red dashed lines indicate the accuracy of 0.5 which is a random guess. IBS, irritable bowel syndrome.

and **1B**). Similar results were observed on an independent dataset (AUROC: 0.886 ± 0.001 [HEAL2] vs. 0.528 ± 0.005 [HEAL]; AUPRC: 0.944 ± 0.001 [HEAL2] vs. 0.709 ± 0.004 [HEAL]; **Supplementary Fig. 1C** and **1D**). These data confirmed the superiority of HEAL2 in genetic risk prediction in the context of nonlinear G2P.

To evaluate the performance of HEAL2 on real ME/CFS data, we first carried out a five-fold cross-validation (5-CV) based on the discovery cohort (**Methods**). Performance variance was estimated by repeating the 5-CV 100 times using different random seeds controlling dataset split and model initialization. We benchmarked HEAL2 against HEAL as our baseline using the same 5-CV procedure. Prediction performance was measured using the area under the receiver operating characteristic curve (AUROC) and the area under the precision-recall curve (AUPRC). Overall, HEAL2 exhibited better prediction performance (AUROC : 0.677 [mean] ± 0.007 [95% CI]; AUPRC: 0.727 ± 0.006; **Fig. 1B**, **Supplementary Fig. 2A**) than HEAL (AUROC: 0.668 ± 0.005; AUPRC: 0.716 ± 0.004; **Fig. 1B**, **Supplementary Fig. 2A**), suggesting that gene interactions might be a significant contributor to ME/CFS pathogenesis. Of note, a logistic regression model using the first 10 principal components (PCs) as its features yielded nearly random prediction (AUROC: 0.518 ± 0.002; AUPRC: 0.586 ± 0.002; **Fig. 1B, Supplementary Fig. 2A**), indicating the population homogeneity of our cohort after QCs.

Next, we evaluated HEAL2 based on the independent Cornell cohort wherein the model was trained on the discovery cohort (**Methods**). This train-test procedure was repeated 500 times with different random seeds. Notably, HEAL2 yielded comparable prediction performance (AUROC: 0.670 ± 0.003; AUPRC: 0.763 ± 0.002; **Fig. 1C**, **Supplementary Fig. 2B**) with that of 5-CV, and substantially outperformed HEAL (AUROC: 0.546 ± 0.005; AUPRC: 0.675 ± 0.004; **Fig. 1C**, **Supplementary Fig. 1B**). This result highlights the superiority of HEAL2 in generalizability over HEAL, indicating that HEAL2 captured biology-relevant genetic factors contributing to ME/CFS.

HEAL2 risk score correlates with ME/CFS-relevant symptoms

Given the phenotypic heterogeneity of ME/CFS patients, we further asked whether our genetic risk score could precisely characterize diverse ME/CFS symptoms and severity. In particular, we linked HEAL and HEAL2 scores to various symptoms measured for ME/CFS patients within the CureME cohort (**Supplementary Table 1**; **Methods**). Surprisingly, we observed that although detailed phenotype data were not seen by the model, HEAL2 risk score was still strongly correlated with many symptoms showing different aspects of ME/CFS manifestation and disease severity (**Fig. 1D**), such as unrefreshing sleep, brain fog, malaise after exertion, and

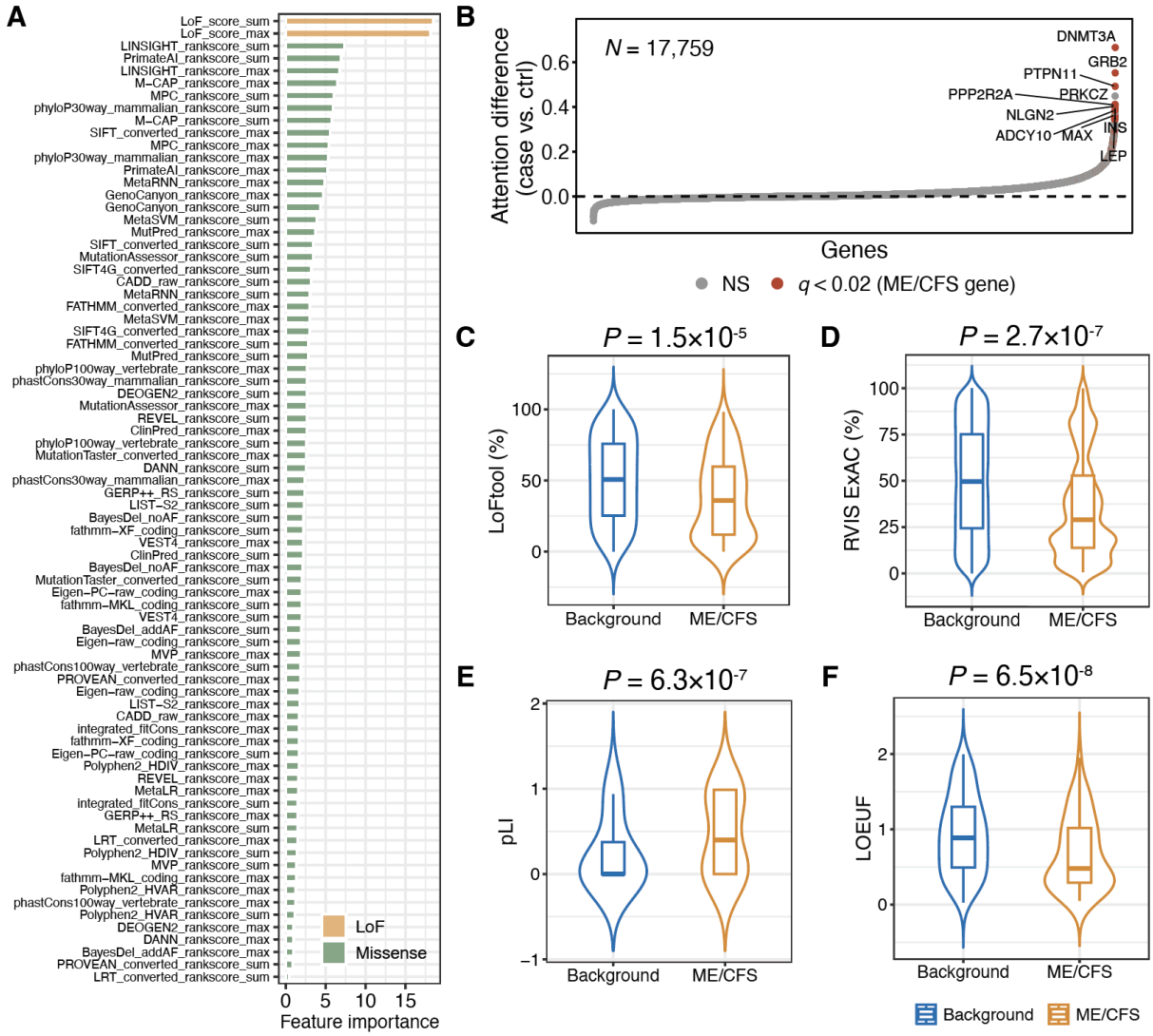

Figure 2. HEAL2 model interpretation and intolerance to LoF variants for ME/CFS genes. (A) HEAL2 input feature importance. LoF, loss-of-function. (B) Gene prioritization by HEAL2 based on attention scores. Ctrl, control; NS, not significant. *q*-value by the Storey-Tibshirani procedure. Top 10 significant genes were highlighted in red. (C-D) Intolerance to LoF variants for ME/CFS genes based on LoFtool (C), RIVS (D), pLI (E), and LOEUF (F). The box plot center line, limits, and whiskers represent the median, quartiles, and 1.5x interquartile range (IQR), respectively. pLI, probability of loss-of-function intolerance; LOEUF, loss-of-function observed/expected upper bound fraction. *P*-value by the two-sided Wilcoxon rank-sum test.

muscle discomfort. Of note, the HEAL2 score yielded sharper correlation than the HEAL score, implicating that HEAL2 better captured the phenotypic variation.

HEAL2 identifies 115 ME/CFS risk genes

Model interpretation enables us to extract biological insights from the trained model. We first assessed the importance of different variant categories and scores in their contribution to prediction (**Methods**). Not unexpectedly, LoF variants, including stop gain/loss, start loss, and frameshift indels, contributed most to prediction (**Fig. 2A**), consistent with previous findings on the larger effect size of LoF variants compared to missense variants[13,14]. This was followed by

evolution-based functional scores for missense variants (**Fig. 2A**), such as LINSIGHT[15] and PrimateAI[16].

Gene-level attention scores derived from HEAL2 inform disease-gene associations. Using simulations, we first demonstrated that HEAL2 precisely prioritized disease-causing genes based on the gene-level attention (AUROC: 0.959; AUPRC: 0.505; **Supplementary Fig. 1E** and **1F**; **Methods**). For ME/CFS, HEAL2 prioritized 115 genes that presented consistently larger attention scores among patients compared to controls (q-value < 0.02, Storey-Tibshirani procedure[17]; **Fig. 2B**, **Supplementary Table 2**; **Methods**). We defined these 115 genes as HEAL2-identified ME/CFS risk genes throughout this study. To gain insights into gene function, we first examined the sensitivity to LoF variants for HEAL2 ME/CFS genes based on four scores (**Methods**), including LoFtool[18], RIVS[19] (derived from the ExAC cohort[20]), pLI[20], and LOEUF[21]. Interestingly, we found that ME/CFS risk genes exhibited significantly stronger intolerance to LoF variants compared to all protein-coding genes (P < 0.05, two-sided Wilcoxon rank-sum test; **Fig. 2C-2F**), suggesting their functional importance in shaping human health.

ME/CFS genes display functional diversity across human tissues and cell types

To dissect the functional heterogeneity of HEAL2 ME/CFS genes, we next sought to systematically examine their expression patterns across different human tissues. By comparing expression levels between ME/CFS genes and the background transcriptome[22] (**Methods**), we observed higher expression of ME/CFS genes spanning multiple tissues (adjusted P < 0.05, two-sided t-test with Bonferroni correction; **Fig. 3A**), including cerebral cortex, skeletal muscle, and colon. To obtain a finer-resolution, we further analyzed single-cell RNA-seq data[22] (**Methods**) and revealed higher expression of ME/CFS genes across various cell types (adjusted P < 0.05, two-sided t-test with Bonferroni correction; **Fig. 3B**), including neurons, smooth muscle cells, and immune cells. At the protein level[23] (**Methods**), we confirmed the higher expression of ME/CFS genes (P < 0.05, two-sided t-test; **Fig. 3C**) within the central nervous system (CNS). These results are consistent with tissues and organs affected by ME/CFS[24,25], implicating their causal roles in impacting the disease risk and symptoms.

To investigate the function of our ME/CFS genes at a systems level, we further carried out a network analysis[12,26–29] (**Methods**) by mapping 115 ME/CFS genes onto a protein-protein interaction (PPI) network[30]. We assessed the enrichment of ME/CFS genes within different gene modules of the PPI network. Notably, four gene modules (out of 1,261 modules) were identified to be significantly enriched with ME/CFS genes (false discovery rate [FDR] < 0.05, Fisher's exact test; **Fig. 4A** and **4B**, **Supplementary Fig. 3**). Gene ontology (GO) analysis showed that M9 genes were associated with proteasome function and particularly degradation of ubiquitinated proteins that are targeted for turnover (**Fig. 4C**), and M20 genes were linked to synaptic function (**Fig. 4D**). These findings reveal the functional diversity of ME/CFS risk genes.

ME/CFS genes are differentially expressed in multiple conditions

Having uncovered the important role of ME/CFS genes in normal tissues and cell types, we next aimed to assess their functional change in diseases, especially ME/CFS.

We first examined the protein expression of our ME/CFS genes based on a previously generated plasma proteome dataset[31]. Of the 115 genes, 57 corresponding proteins were

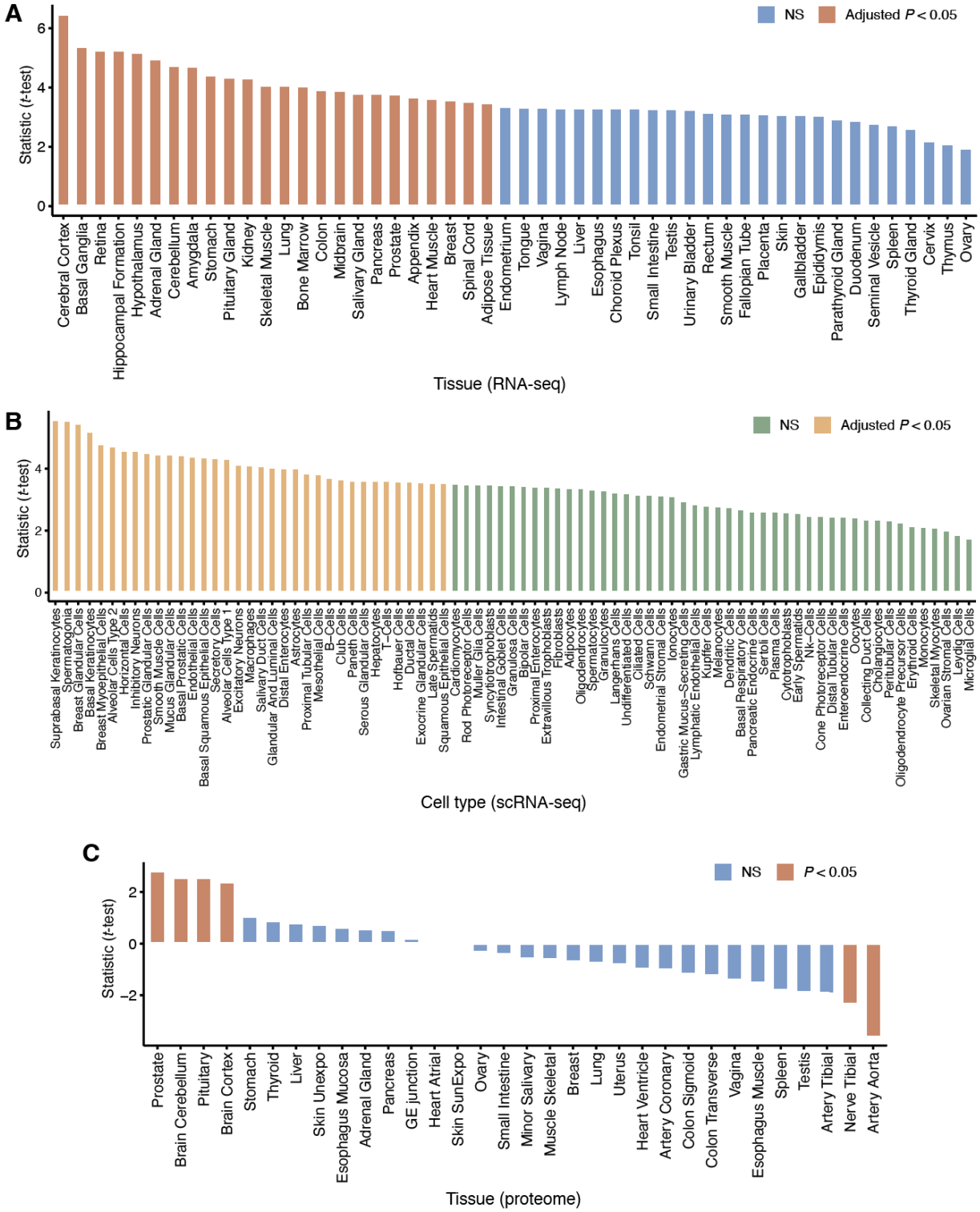

Figure 3. Expression patterns of ME/CFS genes across different human tissues and cell types. (A-B) Gene expression comparison between ME/CFS genes and the transcriptome within 50 human tissues (A) and 81 cell types (B). NS, not significant. *P*-value by two-sided *t*-test. Multiple testing correction was performed using the Bonferroni procedure. (C) Protein expression comparison between ME/CFS genes and all protein-coding genes within 32 human tissues. *P*-value by two-sided *t*-test.

measured in plasma of 20 ME/CFS subjects and 20 controls. We used gene set enrichment analysis (GSEA), which assesses if gene sets are significantly altered as a group, to determine if the ME/CFS genes or the significant modules were also dysregulated in ME/CFS patients compared to controls at the protein level. We found that the protein levels in module M9 (**Fig. 4A**) were significantly decreased in ME/CFS patients versus controls (adjusted $P < 0.002$, normalized enrichment score (NES) = -1.75; **Fig. 4E**). Of the nine ME/CFS genes in M9, four proteins were measured. Two of these, PSMB4 and PSMB5 (components of the 20S core proteasome complex), were part of the leading edge subset (i.e., the proteins that contributed the most to the enrichment signal). The 115 ME/CFS genes and other modules did not show significant enrichment (**Supplementary Fig. 4**).

We also investigated the expression patterns of ME/CFS genes across multiple blood cell types within ME/CFS patients using an RNA-seq dataset[32] generated by Comella et al. Although no difference in expression of overall ME/CFS genes was observed (**Supplementary Fig. 5A**), ME/CFS genes within module M9 (**Fig. 4A**) were markedly down-regulated specifically in patient B cells and T cells compared to those from healthy samples (adjusted $P < 0.05$, two-sided Wilcoxon rank-sum test followed by Bonferroni correction; **Fig. 4F**; **Methods**), showing concordance with the protein dataset and underscoring their cell-type-specific disease relevance. As a negative control, no other module ME/CFS genes were differentially expressed within any patient cell types ($P > 0.05$, two-sided Wilcoxon rank-sum test; **Supplementary Fig. 5B-D**).

To explore the functional changes of the 115 ME/CFS genes with increased granularity, we performed GSEA in cell subsets generated with high resolution clustering of T lymphoid cells from single-cell RNA sequencing (scRNA-seq) of PBMCs derived from ME/CFS patients and controls[33,34] (**Supplementary Fig. 6**). Starting with data from the T cell subset pseudobulked by sample and cell cluster, we again compared expression levels in ME/CFS versus controls for the 115 genes and significant modules. Due to the sparsity of scRNA-seq data, we filtered the genes included in the GSEA to the top quartile to avoid comparing low count genes between groups. Strikingly, the set of 115 ME/CFS genes were significantly downregulated in the cytotoxic CD4 T cell cluster (adjusted $P < 0.02$, NES = -1.77; 61/115 genes were included in GSEA; **Fig. 4G-H)**, identified as such due to its substantially higher expression of effector genes like *CCL5* and *GZMA* compared to conventional CD4 T cell subsets[35] (**Fig. 4I**). 18 of these genes were found in the core enrichment driving the downregulation in ME/CFS patients (**Supplementary Table 3**). Although we did not find significant downregulation of M9 in any of these T lymphoid cell clusters, *SHARPIN* and *PSMD7*, both members of M9, were among the highest ranked genes driving enrichment. Other notable leading edge genes contributing to downregulation in ME/CFS patients include *DNMT3A*, which had the highest attention difference (case vs. controls) in the HEAL2 model, and *PTPN11,* which was ranked third.

To obtain insights into the functional role of ME/CFS genes in other diseases, we systematically analyzed blood RNA-seq data for 59 diseases[22]. Notably, the genes we associated with ME/CFS genes tended to be down-regulated in immunological and infectious diseases ($P < 0.05$, two-sided *t*-test; **Supplementary Fig. 7**; **Methods**), including streptococcal soft tissue infection, pneumococcal pneumonia, pediatric systemic inflammatory disease, and staphylococcus

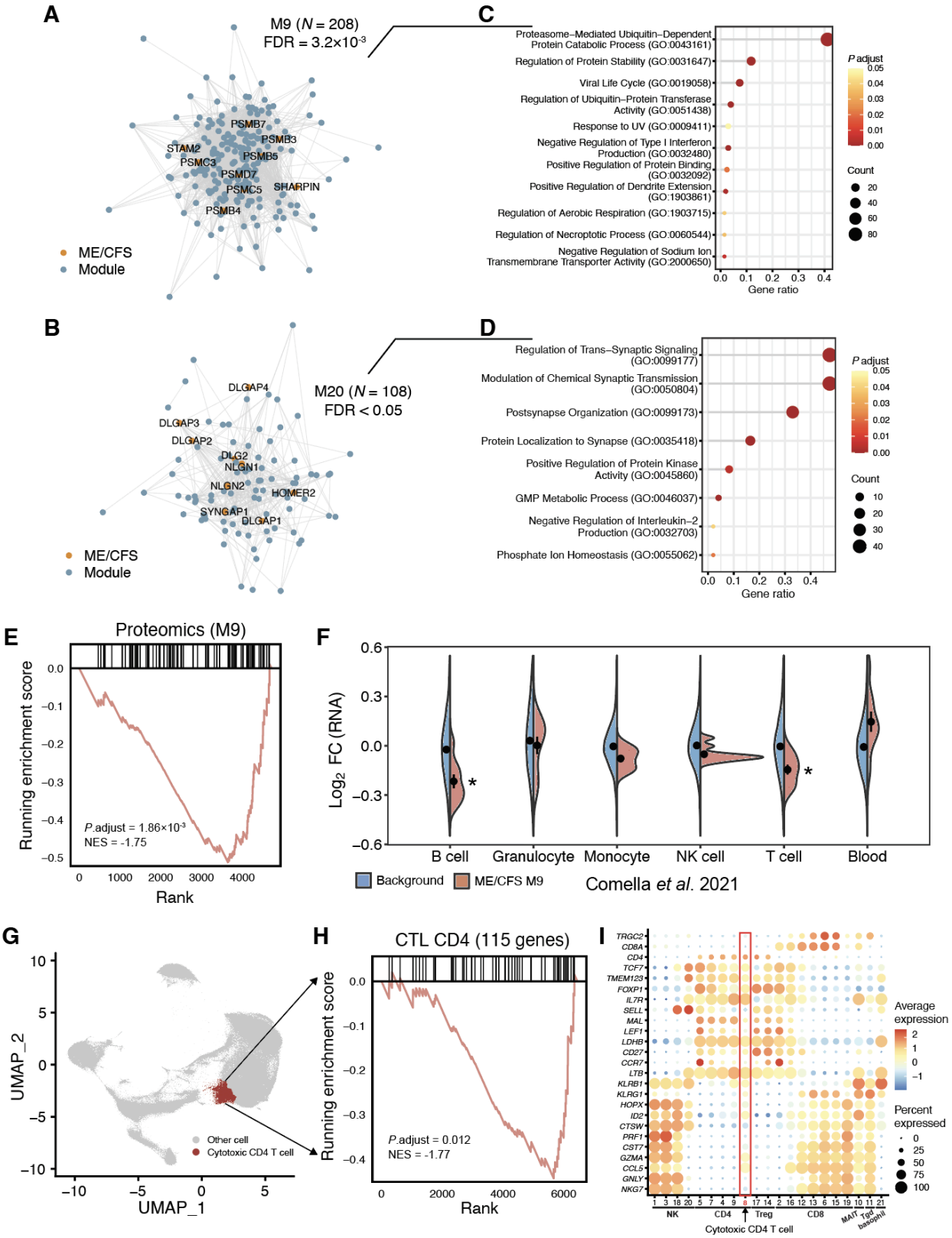

Figure 4. Network dissection and multi-omic analysis of ME/CFS genes. (A-B) Gene modules, including M9 (A) and M20 (B), enriched with ME/CFS genes. FDR, false discovery rate. *P*-value by Fisher's exact test. (C-D) Gene

ontology (GO) analysis (biological process) for M9 (C) and M20 (D) genes. Redundant GO terms were removed using the "simplify" function provided by "clusterProfiler"[36]. GO terms with adjusted $P < 0.05$ were visualized. *P*-value by two-sided Fisher's exact test. (E) GSEA running enrichment plot of plasma proteomics against M9 genes. Negative enrichment score indicates downregulation in ME/CFS and vice versa. GSEA, gene set enrichment analysis; NES, normalized enrichment score. (F) Gene expression comparison for M9 ME/CFS genes between patients and healthy individuals across multiple blood cell types. Dot and error bar represent mean and standard error, respectively. *P*-value by two-sided Wilcoxon rank-sum test followed by Bonferroni correction. FC, fold change; NK, natural killer; *, adjusted $P < 0.05$. (G) Uniform Manifold Approximation and Projection (UMAP) plot of scRNA-seq data, with the cytotoxic CD4 T cell cluster highlighted in red. (H) GSEA running enrichment plot of ME/CFS genes in scRNA-seq pseudobulk data from the cytotoxic CD4 T cell cluster. Negative enrichment score indicates downregulation in ME/CFS cases compared to healthy controls, and vice versa. CTL, cytotoxic T lymphocyte. (I) Relative expression of general, CD4-specific, and cytotoxic T cell marker genes (y-axis) per T cell cluster. Dots represent average expression (color) and percentage of expressing cells (size). Treg, regulatory T cell; mucosal-associated invariant T cell; Tgd, gamma delta T cell.

aureus bacteremia. This result, along with the negative correlation between HEAL2 risk score and fewer viral infections (**Fig. 1D**), implies linkage between infection and ME/CFS[6].

These data together reinforce the implication of LoF in ME/CFS risk genes as potential upstream risk factors for ME/CFS.

Genetic correlation between ME/CFS and other diseases

Patients with ME/CFS often exhibit symptoms that overlap with other conditions, and co-morbidities are commonly observed. This led us to question whether these co-morbidities contribute to the underlying disease mechanism or are downstream effects of pathogenesis. To investigate this, we systematically mapped the genetic correlations between ME/CFS and other complex or Mendelian disorders.

First, leveraging rare variant association studies[37] for 4,529 diseases and traits in the UK Biobank (UKBB), we assessed the distribution of SKAT-O *P*-values of our ME/CFS genes per disease or trait (**Methods**), defining a genetic correlation if this distribution was significantly shifted from the background. Notably, we found that ME/CFS was genetically correlated with various complex diseases and traits in rare variants ($P < 0{,}05$, one-sided Wilcoxon rank-sum test; **Fig. 5A**), including depression, irritable bowel syndrome (IBS), and COVID-19 susceptibility (C2). Similar results were obtained based on the burden tests[37] (**Fig. 5B**). Our results provide a rare-variant-based genetic linkage between ME/CFS and depression.

Next, we explored the common-variant-based genetic correlations based on the genome-wide association studies (GWASs) on 61 complex diseases and traits using a similar procedure (**Methods**). Interestingly, ME/CFS exhibited the strongest genetic correlation with sleep duration (adjusted $P < 0.05$, one-sided Wilcoxon rank-sum test followed by Bonferroni correction; **Fig. 5C**). When linked to COVID-19 phenotypes, we observed a significant common-variant-based genetic correlation between ME/CFS and long COVID-19[38] (strict case definition; $P < 0.05$, one-sided Wilcoxon rank-sum test; **Fig. 5D**; **Methods**). This result is consistent with the symptom similarities between long COVID-19 and ME/CFS[39,40], but provides a genetic perspective.

Finally, we investigated the genetic overlap between ME/CFS and 16 Mendelian disorders. In particular, we estimated the enrichment of ME/CFS genes within different Mendelian disease gene sets[41] (**Methods**), where two disorders including neurologic disorder, and bone and uric

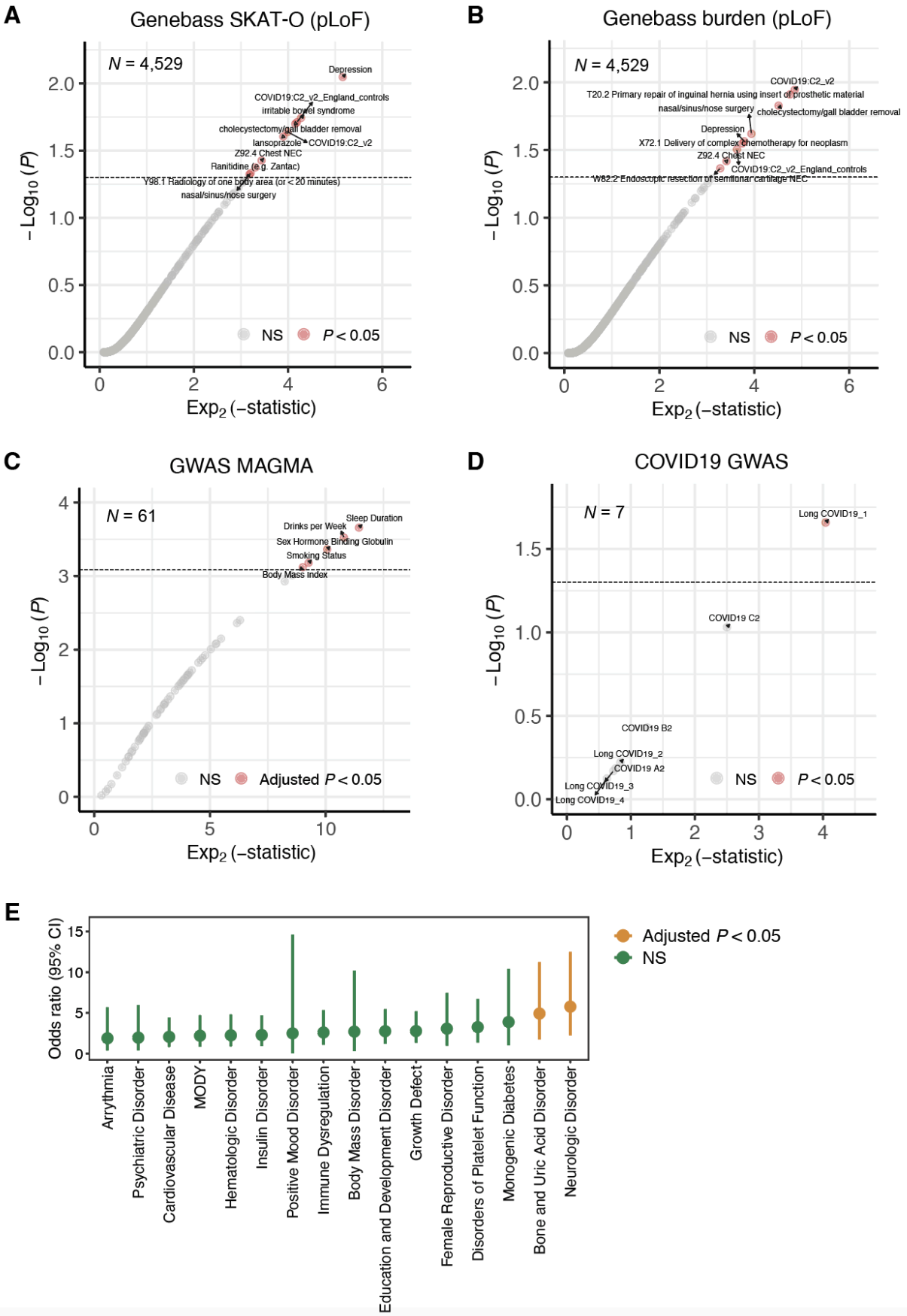
A
Genebass SKAT-O (pLoF)
N = 4,529
Depression
COVID19:C2_v2_England_controls
irritable bowel syndrome
cholecystectomy/gall bladder removal
lansoprazole
COVID19:C2_v2
Z92.4 Chest NEC
Ranitidine (e.g. Zantac)
Y98.1 Radiology of one body area (or < 20 minutes)
nasal/sinus/nose surgery
NS
P < 0.05
−Log10 (P)
Exp2 (−statistic)
B
Genebass burden (pLoF)
N = 4,529
COVID19:C2_v2
T20.2 Primary repair of inguinal hernia using insert of prosthetic material
nasal/sinus/nose surgery
cholecystectomy/gall bladder removal
Depression
X72.1 Delivery of complex chemotherapy for neoplasm
Z92.4 Chest NEC
COVID19:C2_v2_England_controls
W82.2 Endoscopic resection of semilunar cartilage NEC
NS
P < 0.05
−Log10 (P)
Exp2 (−statistic)
C
GWAS MAGMA
N = 61
Sleep Duration
Drinks per Week
Sex Hormone Binding Globulin
Smoking Status
Body Mass Index
NS
Adjusted P < 0.05
−Log10 (P)
Exp2 (−statistic)
D
COVID19 GWAS
N = 7
Long COVID19_1
COVID19 C2
COVID19 B2
Long COVID19_2
COVID19 A2
Long COVID19_3
Long COVID19_4
NS
P < 0.05
−Log10 (P)
Exp2 (−statistic)
E
Odds ratio (95% CI)
Adjusted P < 0.05
NS
Arrythmia
Psychiatric Disorder
Cardiovascular Disease
MODY
Hematologic Disorder
Insulin Disorder
Positive Mood Disorder
Immune Dysregulation
Body Mass Disorder
Education and Development Disorder
Growth Defect
Female Reproductive Disorder
Disorders of Platelet Function
Monogenic Diabetes
Bone and Uric Acid Disorder
Neurologic Disorder

Figure 5. Genetic correlation between ME/CFS and other diseases and traits. (A-B) Rare-variant-based genetic correlation based on SKAT-O (A) and burden (B) tests. *P*-value by one-sided Wilcoxon rank-sum. pLoF, predicted loss-of-function; NS, not significant. (C-D) Common-variant-based genetic correlation based on GWAS for complex diseases and traits (C) and COVID-19 phenotypes (D). Bonferroni procedure was used for adjusting *P*-values. COVID19 A2, B2, and C2 indicates severe covid vs. population, hospitalized covid vs. population, and covid vs. population[42], respectively; long COVID19_1, long COVID19_2, long COVID19_3, and long COVID19_4 indicate strict case vs. broad control, broad case vs. broad control, strict case vs. strict control, and broad case vs. strict control[38], respectively. (E) Genetic correlation between ME/CFS and Mendelian disorders. *P*-value by Fisher's exact test followed by Bonferroni correction. NS, not significant; CI, confidence interval; MODY, maturity-onset diabetes of the young. The dot and error bar indicate the odds ratio and 95% CI, respectively.

acid disorder displayed significant overlaps with ME/CFS (adjusted $P < 0.05$, two-sided Fisher's exact test followed by Bonferroni correction; **Fig. 5E**).

ME/CFS genes reveal diverse disease-relevant mechanisms

Multiple genes prioritized by HEAL2, including *ACE*, *NAMPT*, and *IL12A*, are of biological and therapeutic relevance to ME/CFS pathology. *ACE* plays a critical role in vascular function and immune modulation, with any dysregulation impacting blood flow, inflammation and autonomic function, all of these are implicated in driving ME/CFS pathophysiology[43]. *ACE* has been linked to long COVID-19 and other post-viral syndromes[44]. Furthermore, the availability of well-established ACE modulators[45] could alleviate vascular and inflammatory symptoms, making it an actionable target to pursue. *NAMPT*, contributing to significant downregulation of the 115 ME/CFS genes in cytotoxic CD4 T cells (**Fig. 4G**), is well-established as pivotal in NAD+ biosynthesis and linked to fatigue and mitochondrial dysfunction[46] . This role of *NAMPT*, linking mitochondrial function, energy metabolism, and immune regulation, indicates that treatments involving NAD metabolism warrant further investigation[47]. IL12A is a key cytokine in pro-inflammatory and Th1 immune responses, with dysregulation tied to immune abnormalities in ME/CFS and long COVID-19[48]..

Additionally, we also emphasize the relevance of *PSMB4, PSMB5*, *PSMB7*, *PSMD7, DNMT3A*, *NME1*, *NRAS* and *SYNGAP1* to the pathophysiology of ME/CFS. PSMB4, PSMB5, PSMB7, and PSMD7, all proteasome subunits, are integral to antigen processing and immune regulation, making them highly relevant to ME/CFS's immune dysfunction and persistent inflammation[49]. In our GSEA analyses, PSMB4 and PSMB5 proteins were driving downregulation of functional module M9 (**Fig. 4A**) in plasma of ME/CFS patients versus controls, while *PSMD7* contributed to downregulation of the 115 ME/CFS genes in cytotoxic CD4 T cells (**Fig. 4E** and **4G**). Targeting the proteasome complex using proteasome modulators offers potential for modulating immune responses and alleviating systemic inflammation[50]. *NME1* is directly involved in mitochondrial function and systemic energy production[51]. *NRAS*, via RAS/MAPK signaling, ties into immune dysregulation and chronic inflammation, presenting a potential pathway for anti-inflammatory interventions[52].

As highlighted in our network analysis, ME/CFS genes participate in biological pathways associated with synaptic function (M20; **Fig. 4B** and **4D**). *SYNGAP1,* another gene driving downregulation of the ME/CFS genes in cytotoxic CD4 T cells (**Fig. 4G**) and a member of M20, is involved in synaptic signaling and plasticity, essential for brain function with mutations linked to neurodevelopmental and psychiatric disorders[53]. *SYNGAP1*'s role in synaptic signaling highlights its potential connection to neurological symptoms in ME/CFS, offering therapeutic

potential in neuroprotective strategies[54]. Neuroligins NLGN1 and NLGN2[55], DLG2[56], GRM1[57], and the DLGAP family including DLGAP1, DLGAP2, DLGAP3, and DLGAP4[58] are proteins that regulate synaptic function and glutaminergic synaptic function in particular. Both the neuroligins and the DLGAP proteins are postsynaptic proteins with a role in synapse organisation[59]. Neuroligins bind to presynaptic neurexins and have a role in synapse specification. This entire set of synaptic genes has been linked to various neuropsychiatric disorders including clinical depression[59]. *NRGN1* was the only genome-wide significant hit in a GWAS of suicide behaviour that is linked to major depression[60]. A truncating LoF mutation within *NRGN1* has been linked to depression in the context of familial Alzheimer's disease[61]. Most prominently, this set of synaptic genes is implicated in attention deficit hyperactivity disorder (ADHD) and autistic spectrum disorder (ASD) (Wikipathways WP5420). Indeed the entire set of ME/CFS genes is significantly enriched in this pathway ($P = 3.9 \times 10^{-10}$, two-sided Fisher's exact test). A shared genetic basis between ME/CFS and ADHD/ASD suggests that these two disorders may have shared aspects of molecular dysfunction. It is intriguing that the typical age of onset of ADHD/ASD is in childhood whereas ME/CFS typically manifests in adolescence or adulthood[62]. If both disorders share a related mechanism then perhaps they are age-specific manifestations of a similar underlying process.

Collectively, this expanded gene set integrates immune, metabolic, and neurological mechanisms, providing a multifaceted framework for understanding ME/CFS pathology and potential for developing targeted therapeutic interventions.

Discussion

Our study represents a significant advancement in the understanding of the genetic underpinnings of ME/CFS. We conducted a large whole-genome sequencing analysis of ME/CFS by applying a novel deep learning framework, HEAL2. By leveraging whole genomes from multiple cohorts for rare variant analysis, we identified 115 risk genes associated with ME/CFS, many of which exhibit significant intolerance to loss-of-function mutations, which is corroborated using evidence from patient multi-omics analysis. These risk genes play critical roles in diverse tissues, including the central nervous system and immune system, aligning with the multisystemic nature of the disease[63]. Collectively, our study provides novel insights into the genetic etiology of ME/CFS and also highlights the power of integrating genome-wide data with machine learning approaches for rare variant analysis.

Our findings build upon earlier studies suggesting a genetic susceptibility in ME/CFS, and substantially extend this knowledge from prior studies, which were often constrained by small sample sizes and inconsistent methodologies. By employing whole-genome sequencing and integrating advanced computational methods like HEAL2, we have overcome many limitations of earlier research. HEAL2 identified 115 risk genes that exhibit intolerance to loss-of-function mutations and emphasizes the potential role of these genes in maintaining cellular and systemic homeostasis. This intolerance to loss-of-function mutations provides information about underlying disease mechanisms contributing to the pathogenesis of ME/CFS and experimentally validating these insights will open avenues for targeted therapeutic interventions aimed at modulating these pathways.

Network analyses further revealed these ME/CFS risk genes' roles in diverse cellular processes and implicated multiple tissues in disease pathogenesis. Functional analysis uncovered significant expression of ME/CFS genes in critical tissues, such as the central nervous system (CNS), skeletal muscle, and immune cells. Overall, these findings align with the clinical manifestations of ME/CFS, including cognitive impairment, fatigue, and immune dysfunction.

The downregulation of ME/CFS genes and the differential expression patterns observed from patient multi-omics data support their functional relevance to disease mechanisms and their potential to be identified as potential therapeutic targets. Moreover, based on HEAL2-identified ME/CFS genes we uncovered genetic correlations between ME/CFS and conditions such as depression and long COVID-19 susceptibility. This result aligns with a recent GWAS[64] linking long COVID-19 to depression and ME/CFS. These correlations offer a genetic rationale for observed clinical overlaps and suggest shared pathophysiological mechanisms, potentially rooted in immune and neuroinflammatory pathways.

HEAL2 extends our previous work of HEAL[12], which is a rare-variant-based genetic risk predictor. Different from HEAL, HEAL2 extensively explores PPIs which could contribute to disease risk in addition to linear genotype-phenotype (G2P) relationships. We demonstrated, in the context of ME/CFS, HEAL2 significantly outperformed HEAL in disease prediction, which implies that the nonlinear gene interactions may shape a considerable genetic architecture of ME/CFS. In our recent work[65], we also proved that the incorporation of PPIs could improve genetic risk prediction based on common variants.

Given the well-established interpretation of the coding variants, in this study we only focused on missense and LoF variants in the analysis. However, noncoding variants, which account for a large proportion of human genetic variants, are missing in our current modeling. It is still a challenge in the field[66], compared to coding variants, to interpret the function of noncoding genomes and variants, given their functional heterogeneity and dynamics across different tissues and conditions[67]. On the other hand, HEAL2 can be easily extended to incorporate noncoding variants in disease prediction, if the noncoding variant effects and their target genes are well defined. We anticipate that, along with the progress in the study of noncoding variants, HEAL2 could be applied to model G2P more comprehensively by integrating both common and rare, coding and noncoding variants.

Although gene discovery power has been enhanced by our machine learning modeling, the generalizability and stability of genetic risk prediction need further validation on additional independent cohorts. In this study, we only focused on European samples using a stringent cutoff, aiming to remove latent population-related genetic factors that could bias our biological discovery. However, it is well known that the genetic architecture of complex diseases and traits diverge among populations[68]. Thus it remains an open question whether the same conclusions hold for ME/CFS patients from other diverse populations. The solution of this question requires future work that focuses on including non-EUR ME/CFS cohorts.

This study highlights the power of integrating machine learning with genomics for understanding complex diseases. HEAL2 not only identifies genetic factors contributing to ME/CFS but also provides a framework for rare variant analysis applicable to other complex heterogeneous conditions. The identification of specific genetic variants and pathways involved in ME/CFS

pathogenesis has important clinical implications for diagnostics and therapeutics. This knowledge could accelerate the discovery of biomarkers and therapeutic targets, moving toward precision medicine for ME/CFS and related disorders. The genetic correlations with other diseases suggest promising avenues for repositioning existing therapies or developing targeted treatments that address these overlapping mechanisms. More experimental follow-ups are needed to confirm our data-driven implications.

In conclusion, our study provides a genetic characterization of ME/CFS and reveals novel insights into its pathophysiology. The HEAL2 framework offers a robust analytical framework for rare variant analysis, promising to enhance our understanding of complex diseases.

Acknowledgements

We are sincerely grateful for all research participants, including ME/CFS patients and healthy individuals, for their involvement and dedication. This study was carried out using samples from the CureME and UK ME/CFS Biobank (REC reference 21/WA/0388 to M.P.S.), which were processed and stored at the UCL-RFH BioBank. This study is supported by the Candace & Bert Forbes gift funds (to M.P.S.). M.J.Z. acknowledges the support of the Shurl and Kay Curci Foundation.

We thank the following individuals who participated in one or more of these activities to acquire the Cornell samples – participant screening, participant assessment, blood collection, data curation: Victoria Birdsall, John Chia, Patricia Doty, Carl Franconi, Tiffany Ong, Betsy Keller, Susan Levine, Xiangling Mao, Geoffrey Moore, Maria Russell, Dikoma Shungu, Jared Stevens, Kristin Treat, and David Wang.

NIH U54NS105541, an initial grant provided to the Cornell ME/CFS Collaborative Research Center, was co-funded by the National Institute of Neurological Disorders and Stroke, National Institute of Allergy and Infectious Diseases (NIAID), National Institute on Drug Abuse, National Heart, Lung, and Blood Institute, National Human Genome Research Institute, and the Office of the Director. A renewal grant was made to the Cornell Center from NIH NIAID: U54AI178855.

Author Contributions

S.Z. and M.P.S. conceived and designed the project. S.Z., and M.K. designed HEAL2. M.K. implemented HEAL and HEAL2 with assistance from H.L. Sample preparation and processing was conducted by T.C. V.C. carried out data preprocessing, quality controls, and ancestry analysis. F.J. provided part of the Stanford samples. M.R.H. and A.G. provided the Cornell samples. M.L. and M.J.Z. performed MAGMA analysis. S.Z., M.K., V.C., K.A.G. and D.S.I. performed data analysis with the help from all other authors. All authors are responsible for data interpretation. M.P.S. and S.Z. supervised the project. S.Z., V.C., M.K., and K.A.G. prepared the manuscript with the help from all other authors.

Competing Interests

M.P.S is a cofounder and scientific advisor of Crosshair Therapeutics, Exposomics, Filtricine, Fodsel, iollo, InVu Health, January AI, Marble Therapeutics, Mirvie, Next Thought AI, Orange Street Ventures, Personalis, Protos Biologics, Qbio, RTHM, SensOmics. M.P.S. is a scientific

advisor of Abbratech, Applied Cognition, Enovone, Jupiter Therapeutics, M3 Helium, Mitrix, Neuvivo, Onza, Sigil Biosciences, TranscribeGlass, WndrHLTH, Yuvan Research. M.P.S. is a cofounder of NiMo Therapeutics. M.P.S. is an investor and scientific advisor of R42 and Swaza. M.P.S. is an investor in Repair Biotechnologies.

M.R.H. is a member of the scientific advisory boards of the Open Medicine Foundation, Solve CFS/ME, the WE&ME Foundation, and Simmaron Research.

Supplementary Figures

Supplementary Figure 1. Simulation results. (A-B) Prediction performance of five-fold cross-validation (100 repeats), evaluated using the receiver operating characteristic (ROC) curve (A) and the precision-recall curve (B). The curve and shaded area represent the AUROC mean and 95% confidence interval (CI), respectively. (C-D) Prediction performance of testing (500 repeats) on an independent dataset, evaluated using the ROC curve (C) and the precision-recall curve (D). (E-F) Performance of HEAL2 gene prioritization, evaluated using the ROC curve (E) and the precision-recall curve (F). The labels of 100 genes selected to generate the disease status in simulation were 1, and the rest of genes were labeled as 0.

Supplementary Figure 2. Prediction performance evaluation in precision-recall curve. (A) Prediction performance of five-fold cross-validation (100 repeats) on the discovery cohort. The curve and shaded area represent the AUPRC mean and 95% confidence interval (CI), respectively. AUPRC, area under the precision-recall curve; PC, principal component. (B) Prediction performance of testing (500 repeats) on the independent Cornell cohort. The curve and shaded area represent the AUPRC mean and 95% CI, respectively.

Supplementary Figure 3. Network analysis for ME/CFS genes. (A-B) Gene modules, including M15 (A) and M18 (B), enriched with ME/CFS genes. FDR, false discovery rate. *P*-value by Fisher's exact test. (C-D) Gene ontology (GO) analysis (biological process) for M15 (C) and M18 (D) genes. Redundant GO terms were removed using the "simplify" function provided by "clusterProfiler". GO terms with adjusted $P < 0.05$ were visualized. *P*-value by two-sided Fisher's exact test.

Supplementary Figure 4. Additional proteomics GSEA results for modules (A) M15, (B) M18, (C) M20, and (D) all 115 ME/CFS genes, respectively. GSEA, gene set enrichment analysis; NES, normalized enrichment score.

Supplementary Figure 5. Differential expression analysis of ME/CFS genes based on patient data. (A-D) Expression comparison across multiple blood cell types between cases and controls for all ME/CFS genes (A), M15 ME/CFS genes (B), M18 ME/CFS genes (C), and M20 ME/CFS genes (D), respectively. Dot and error bar represent mean and standard error, respectively. No difference was significant by the two-sided Wilcoxon rank-sum test. NK, natural killer.

Supplementary Figure 6. UMAP plot of the PBMC scRNA-seq dataset for ME/CFS. Cells were clustered and annotated as described elsewhere[34]. UMAP, uniform manifold approximation and projection; PBMC, peripheral blood mononuclear cell; NK, natural killer cell; Th, T helper cell; CTL, cytotoxic T lymphocyte; Treg, regulatory T cell; MAIT, mucosal-associated invariant T cell. The figure was adapted from Iu et al.[34]

Supplementary Figure 7. Gene expression patterns for ME/CFS genes in blood across 59 diseases. NS, not significant. *P*-value by two-sided *t*-test.

Supplementary Tables

Supplementary Table 1. Prediction accuracy of different ME/CFS symptoms within the UK CureME cohort based on HEAL and HEAL2 risk scores. Acc, accuracy.

Supplementary Table 2. Genes prioritized by HEAL2.

Supplementary Table 3. 18 leading edge genes in GSEA of 115 ME/CFS genes in cytotoxic CD4 T cells. GSEA, gene set enrichment analysis.

Methods

Stanford ME/CFS cohort

The Stanford ME/CFS cohort comprises 364 participants (208 cases and 156 controls), including members from 22 families totaling 74 participants, with 9 identical twins discordant for ME/CFS. Participants received ME/CFS diagnoses from specialized clinicians in the Bay Area and underwent comprehensive clinical assessments to confirm diagnoses based on ICC and IOM criteria[69–71]. Detailed phenotypic data were collected for all participants, ensuring a rich dataset for analysis. Blood samples were collected over several years at multiple Stanford locations and, for very severe and extremely severe cases, at patients' homes. Samples were collected using 10 ml K2 EDTA vacutainers, processed immediately, snap-frozen in liquid nitrogen, and stored at -80°C. The research was approved by the Institutional Review Board at Stanford University (40146), adhering to rigorous protocols to ensure high-quality, anonymized data and samples.

We further increased the number of negative controls by incorporating samples from the iPOP (N = 110) and hPOP (N = 268) cohorts which are described elsewhere[72,73]. This yielded the final Stanford ME/CFS cohort including 208 patients and 534 controls.

UK CureME ME/CFS cohort

The UK CureME cohort[74] is a comprehensive resource designed to advance research into ME/CFS and is part of the UK ME/CFS Biobank initiative (https://cureme.lshtm.ac.uk/). Participants undergo thorough clinical assessments to confirm diagnoses and provide detailed phenotypic data. Biological samples, primarily blood, are collected at multiple time points to facilitate longitudinal analyses. The cohort adheres to rigorous protocols to ensure high-quality, anonymized data and samples. From the UK CureME cohort, we received blood samples for 190 individuals with ME/CFS and 30 healthy controls who provided consent for WGS (RFL Biobank Ethical Reference number: NC2021.24). The cohort adheres to rigorous protocols to ensure high-quality, anonymized data and samples, which are stored at the UCL/RFH Biobank in London, UK.

Cornell ME/CFS cohort

The Cornell cohort was composed of 66 individuals with ME/CFS and 47 healthy controls who consented to provide blood for WGS. Almost all were participants in the cohort described by Moore et al.[75], though a few provided blood but did not participate in exercise testing. Subjects visited three different sites for blood collection: ID Med in Torrance, CA; Cornell University and Ithaca College in Ithaca, NY; and Weill Cornell Medicine in New York, NY. Following blood draw into K2 EDTA vacutainers, samples were provided to processing labs at each site. 1 ml whole blood aliquots along with demographic information were provided to Stanford for isolation of DNA. The research was approved by Institutional Review Boards at Cornell University (IRB# 0001855), Ithaca College (IRB# 1017-12D), or Weill Cornell Medicine (IRB# 1708018518).

HEAL2 model specification

To investigate the genetic architecture of ME/CFS, we developed HEAL2, an advanced deep learning framework that integrates graph neural networks (GNNs) with an attention-readout mechanism coupled with a sparse autoencoder (SAE) for interpretability. HEAL2 extends our previous linear model, HEAL[12], by incorporating multidimensional pathogenicity scores and leverages a protein-protein interaction (PPI) network to capture complex, non-additive genetic interactions. Similar to PRS-Net[65], a GNN model but for polygenic risk scores, we first derive our PPI network from the STRING database[30], as protein-protein interactions are good representations of relevant gene-gene associations, selecting only for high confidence (score > 700) links. In detail, we build the graph $\mathcal{G} = (\mathcal{V}, \boldsymbol{E})$, where $\mathcal{V}$ is the set of nodes (genes) while $\boldsymbol{E}$ corresponds to the set of edges (v_i, v_j), representing the interaction between gene i and j as obtained from the STRING database. Next, every node is further extended with a self-loop (v_i, v_i), allowing each gene to retain its own information during message passing, preserving individual gene characteristics alongside interaction effects.

To construct the input features for HEAL2, we began by representing each individual's genetic data through a comprehensive feature vector of the mutational burden across genes. For every gene in each sample, we aggregated the rare missense variants and their corresponding annotated scores by both summing, capturing the cumulative mutational burden for each gene, and taking the maximum pathogenicity score across all variants, highlighting the potential impact of the most deleterious variant. For LoF variants (i.e., start loss, stop gain, stop loss, and frameshift indels), which may lack predicted scores, we also included the gene's probability of being loss-of-function intolerant (pLI) score from gnomAD v.4.1. This process resulted in individual-specific gene feature vectors that capture both the cumulative and peak effects of rare coding variants for each gene across 39 annotated scores. Formally, each gene $v_i \in \mathcal{V}$ is assigned an initial feature vector $\mathbf{h}_i \in \mathcal{H}$, where $\mathcal{H} \in \mathbb{R}^{|\mathcal{V}|\times 78}$ and $|\mathcal{V}|$ is the total number of genes in $\mathcal{G}$. Our input gene feature vectors are first passed through a multilayer perceptron (MLP) to obtain initial gene embeddings:

$$\mathcal{H}^0 = MLP^0(\mathcal{H}), \quad (1)$$

where $\mathcal{H}^0 \in \mathbb{R}^{|\mathcal{V}|\times D}$ and D is the dimension of hidden states.

To capture nonlinear gene-gene interactions within our PPI network, we apply multiple layers of the Graph Isomorphism Network[76] (GIN). These GIN layers execute message-passing operations across the network, progressively updating each node's representation by incorporating information from its neighboring nodes. At each layer k, the representation of gene v_i is updated as follows:

$$\mathbf{h}_i^k = MLP^k((1 + \epsilon^k) \cdot \mathbf{h}_i^{k-1} + \sum_{v_j \in N(v_i)} \mathbf{h}_j^{k-1}), \quad (2)$$

where $\mathbf{h}_i^{k-1}$ represents the hidden state of v_i from the $k - 1$-th layer, $N(v_i)$ denotes the set of neighboring genes in the GGI network, and ϵ^k is a learnable parameter specific to layer k. The

MLP^k transforms the combined information, allowing the model to weigh self-information and neighbor contributions at each layer adaptively. After k iterations, each gene's representation integrates information from genes within its k-hop neighborhood, embedding both local and extended gene interaction patterns.

For model interpretation and prioritizing genes contributing to ME/CFS risk, we employ an attentive readout module integrated with a sparse autoencoder (SAE). The attentive readout focuses on key genes by assigning attention weights, while the SAE refines these features by enforcing sparsity, highlighting the most informative genes. For each sample, the global representation $\mathbf{h}_{graph}$ is first derived through the attention mechanism as follows:

$$\mathbf{h}_{graph} = AttentiveReadout(\mathbf{Q}, \mathbf{K}, \mathbf{V}), \quad (3)$$

where $\mathbf{K} = \mathcal{H}^L \mathbf{W}_{key}$ and $\mathbf{V} = \mathcal{H}^L \mathbf{W}_{value}$ are the key and value matrices derived from the final GNN layer embeddings $\mathcal{H}^L$ using trainable projection matrices $\mathbf{W}_{key} \in \mathbb{R}^{D \times D}$ and $\mathbf{W}_{value} \in \mathbb{R}^{D \times D}$. The attention scores are calculated as:

$$\mathbf{A} = Sigmoid(\mathbf{Q} \cdot \mathbf{K}), \quad (4)$$

where $\mathbf{Q} \in \mathbb{R}^{1 \times D}$ is a trainable query vector, assigning importance to each gene, with higher values in $\mathbf{A}$ indicating greater relevance.

The attention-weighted hidden representations, $\mathbf{A} \cdot \mathbf{V}$, are subsequently passed through the SAE for further refinement. Within the SAE, the encoder maps these attention-weighted hidden features to a sparse latent space:

$$\mathbf{z}_{enc} = ReLU(\mathbf{W}_{enc}(\mathbf{A} \cdot \mathbf{V}) + \mathbf{b}_{enc}), \quad (5)$$

where $\mathbf{W}_{enc}$ and $\mathbf{b}_{enc}$ are the encoder's weights and bias terms. To encourage sparsity, an L_1 penalty is applied to $\mathbf{z}_{enc}$, helping to isolate the most informative genes. The latent representation is then decoded back to the original dimensionality and assigned $\mathbf{h}_{graph}$. The reconstruction error is combined with the sparsity constraint to form the following loss function:

$$L_{SAE} = \left\| \mathbf{A} \cdot \mathbf{V} - \mathbf{z}_{enc} \right\|_2 + \alpha \left\| \mathbf{z}_{enc} \right\|_1, \quad (6)$$

where α is a sparsity regularization coefficient and was set to 1 in this study.

Finally, the graph-level representation $\mathbf{h}_{graph}$, constructed from the SAE-processed embeddings across all nodes, is passed through an MLP, outputting the final ME/CFS classification. The training objective thus combines binary cross-entropy loss for classification and the SAE's sparsity-constrained reconstruction loss, optimizing both prediction accuracy and interpretability. In this study, we used 78 input features to match our annotated scores while the rest of the model parameters were set to those of PRS-Net[65] with 64 hidden dimensions, one gene-encoding layer, one GIN layer, and two predictor layers.

HEAL model specification

To provide a fair comparison between HEAL2 and our previous model, HEAL[12], we slightly extended it to include the multidimensional mutational burden used as input for HEAL2. Specifically, we redesigned HEAL to utilize the comprehensive gene feature vectors that capture both the cumulative and peak effects of rare variants across the 39 annotated scores for each gene. In our modification of HEAL, we employ a linear modeling approach that treats each gene independently, focusing on the aggregated mutational burden per sample without considering gene interactions. Formally, each gene $v_i \in \mathcal{V}$ is assigned an initial feature vector $\mathbf{h}_i \in \mathbb{R}^{78}$, identical to the input in HEAL2. Our model begins by transforming these gene-specific feature vectors into scalar gene scores using a linear transformation:

$$s_i = \mathbf{w}_{feat}^{\top}\mathbf{h}_i + b_{feat}, \quad (7)$$

where $s_i \in \mathbb{R}$ is the score for each gene v_i, $\mathbf{w}_{feat} \in \mathbb{R}$ are the weights applied to the features, and b_{feat} is a bias term. This transformation effectively summarizes the multidimensional mutational burden of each gene into a single scalar value. Next, we aggregate the gene score into a single ME/CFS prediction score y for each sample by applying another linear transformation:

$$y = \mathbf{w}_{gene}^{\top}\mathbf{s} + b_{gene}, \quad (8)$$

where $\mathbf{s} \in \mathbb{R}^{|\mathcal{V}|}$ is the vector of gene scores, $\mathbf{w}_{gene} \in \mathbb{R}$ are the weights assigned to each gene, and b_{gene} is a bias term. As a key feature of the original HEAL model is applying LASSO regularization to force the model to focus on a key set of genes, we further introduce L_1 regularization on both the feature-level weights $\mathbf{w}_{feat}$ and the gene-level weights $\mathbf{w}_{gene}$, resulting in optimizing the final loss function:

$$L = L_{classification} + \lambda_{feat}\left\|\mathbf{w}_{feat}\right\|_1 + \lambda_{gene}\left\|\mathbf{w}_{gene}\right\|_1, \quad (9)$$

where $L_{classification}$ is the binary cross-entropy loss, while λ_{feat} and λ_{gene} are hyperparameters controlling the strength of regularization at the feature and gene levels, respectively. After manual tuning on the validation set, we set $\lambda_{feat} = 0.01$ and $\lambda_{gene} = 0.1$.

Model training and testing

We evaluated HEAL2's ability to predict ME/CFS risk using both cross-validation within the discovery cohort (by combining the Stanford and UK CureME cohorts) and independent testing on the Cornell cohort. First, we applied stratified five-fold cross-validation (5-CV) on the discovery cohort, comprising 247 ME/CFS cases and 192 controls, to ensure that each fold retained the same proportion of cases and controls. This procedure, repeated 100 times with different random seeds, provides robust performance estimates by controlling for variance across different data splits.

The HEAL2 model was implemented in PyTorch with the Deep Graph Library (DGL). We trained the model using the AdamW optimizer, with a learning rate of 6.25×10^{-5}, a batch size of 16 and weight decay of 1×10^{-6}. To prevent overfitting, we employed early stopping, halting the training procedure if performance on the validation set failed to improve over 20 consecutive epochs.

For independent validation, we used the Cornell cohort (36 cases, 21 controls), withheld entirely from model training. Testing was performed when model training was complete on the discovery cohort, once every fold, resulting in 500 total tests on the independent cohort. Performance was evaluated by calculating the area under the receiver operating characteristic curve (AUROC) and the area under the precision-recall curve (AUPRC), with results reported as mean values and 95% confidence intervals across all repetitions.

Additionally, we evaluated the performance of our previous HEAL model using the same training and evaluation protocols for comparison. All experiments were conducted on multiple NVIDIA A100 GPUs.

Simulation details

To validate HEAL2's ability to model nonlinear genotype-phenotype relationships and accurately identify disease-relevant genes, we constructed a synthetic dataset with a “known” set of simulated causal genes. Specifically, we initialized HEAL2 with random, fixed weights and performed a forward pass of all samples to extract their final gene-level representations. From averaging these representations across all samples for each gene, we selected the top 100 genes to act as our ground-truth. We then amplified the influence of these 100 genes by scaling their specific weights in the final representation and repeated the forward pass. The resulting predictions from the model were thresholded at the median to assign simulated case/control status. The resulting synthetic dataset provided a controlled scenario with stable phenotypic labels related to a known set of 100 genes.

We then applied the same performance evaluation and gene prioritization procedures used in the ME/CFS analysis to this synthetic dataset for both HEAL2 and HEAL. To quantify how accurately HEAL2 recovered the artificially designated causal genes, we treated the known set of 100 “injected” causal genes as true positives and computed AUROC and AUPRC by comparing the attention-based gene prioritization against these ground-truth labels.

DNA preparation and sequencing

Genomic DNA was isolated from whole blood using the QIAamp DNA Blood Midi Kit (Qiagen, Cat. No. 51185) following the manufacturer's protocol. One milliliter of whole blood was used for each extraction. The isolated DNA was quantified using the Qubit™ dsDNA Quantification Assay Kit (Thermo Fisher Scientific, Cat. No. Q32851) and stored at -80°C until sequencing. Whole genome sequencing was performed by Novogene using their PCR-free WGS platform. For each sample, 300 ng to 1 µg of total genomic DNA was submitted. Prior to sequencing, all samples underwent rigorous quality control assessments to ensure only high-quality DNA was processed. Each sample was sequenced across 1-5 lanes to obtain more than 90 gigabases (Gb) pairs of reads per sample, and the resulting FASTQ files were concatenated. The

sequencing data were deposited in an Amazon S3 bucket within the Stanford Data Ocean repository for secure storage and access. This comprehensive approach to DNA preparation and sequencing ensures high-quality data for downstream analyses, adhering to best practices in genomic research.

Read alignment and variant calling

The read alignment and variant calling was done using the Sentieon's DNAseq pipeline which adheres to GATK best practices while providing significant computational efficiency and accuracy. The pipeline implements the same mathematics used in the Broad Institute's BWA-GATK HaplotypeCaller 4.0 workflow, but is highly parallelizable and optimized for performance, achieving 10X faster processing speeds for alignment. The pipeline processes data from FASTQ to VCF, completing BAM-to-VCF conversion in under 30 minutes. The pipeline supports extensive QC measures, such as metrics for base quality score distribution, read alignment quality, and duplicate marking, which were integrated seamlessly within the workflow.

Quality controls

Following the best practice[12], quality controls (QCs) for WGS were conducted using PLINK's QC metrics[77] which involves a series of steps to ensure that the data is clean, reliable, and suitable for downstream analysis. Sample-level and variant-level QCs were done where samples were filtered for high rate of genotype missingness, abnormal high or low heterozygosity rates or deviations from Hardy-Weinberg Equilibrium (HWE) to account for errors or poor-quality DNA. Closely related individuals were also filtered out by calculating Identity by Descent (IBD) and relatedness. Pruning was performed and individuals with first or second degree relative in the sample were removed.

Ancestry analysis

Ancestry analysis was performed by leveraging the population structure information obtained from principal component analysis (PCA) using PLINK's Eigensoft tool. PCA is a dimensionality reduction technique used in PLINK to summarize genetic variation into principal components (PCs). These PCs were plotted to visualize population structure, detect ancestry patterns, and spot any population outliers. We also performed population admixture analysis using the ADMIXTURE[78] for ancestry inference and population structure analysis. The 1000 Genomes[79] (1KG) were used as the reference to ADMIXTURE. Samples with EUR estimates $Q > 0.99$ were retained for downstream analysis.

Variant annotation

Variant annotation was performed using Annovar[18]. Variant types, including missense, stop gain, stop loss, start loss, and frameshift indels, were annotated along with their affected genes. Allele frequencies were computed based on gnomAD[21] v4.1. For pathogenicity scores for missense variants, we relied on the dbNSFP database[80] which compiled numerous prediction scores.

Input feature prioritization

HEAL2 evaluates the contribution of specific variant annotations and pathogenicity scores by calculating gradient-based feature importance. During model evaluation on the test set, the gradient of the model's prediction with respect to the input features was computed for each

sample. The absolute gradients were summed across all genes in the GGI network, condensing the overall contribution of each feature into a single importance score. For this analysis, we re-trained HEAL2 on the full cohort (Stanford, UK CureME, and Cornell) using a train-test-split of 80% for training and 20% for validation, repeated over 100 iterations employing the same early-stopping strategy as for the performance evaluation. Mean feature importance scores were computed per sample for each feature across all iterations to ensure stability. These scores were then compared between cases and controls, highlighting the features with the most relevance in regards to the classification.

Gene prioritization

To further interpret HEAL2's predictions, we prioritized genes contributing to ME/CFS risk using the model's attentive readout mechanism. For each sample and gene, we took the absolute sum of the SAE-decoded attention-weighted representations across all hidden dimensions, generating a single score that condenses the gene's contribution to ME/CFS classification. We then averaged these scores per sample across 100 iterations of training on the full cohort. The mean scores for each gene were compared between cases and controls using the Mann-Whitney U test, followed by Storey-Tibshirani adjustment[17] for multiple hypothesis testing (q-value < 0.02). This process identified 115 genes with consistently higher attention scores in cases compared to controls, defining these as HEAL-2 prioritized ME/CFS risk genes.

ME/CFS symptom analysis

To assess the relationship between genetic risk scores and ME/CFS symptoms, we analyzed HEAL2's prediction scores in relation to additional phenotypic data from the UK CureME cohort. Specifically, we focused on the validation sets from the 100 iterations of 5-CV, calculating the mean prediction score for each sample across all iterations where the sample appeared in the validation set. Next, these averaged prediction scores were used to calculate the accuracy in capturing symptom-specific phenotypic variation for each binary phenotype. For comparison, this procedure was repeated using HEAL's prediction scores to evaluate its performance on the same phenotypic data.

LoF intolerance analysis

We used four different scores, including LoFtool[18], RIVS[19], pLI[20], and LOEUF[21], to quantify gene intolerance to LoF variants. Two-sided Wilcoxon rank-sum test was used to compare the scores of ME/CFS genes identified by HEAL2 with those of all background genes.

Differential expression analysis

For differential expression (DE) analysis for baseline human tissues and cell types, we used a two-sided t-test to compare the expression levels of ME/CFS genes identified by HEAL2 with those of all expressed genes. The t-test statistics was used to estimate the expression difference, and the Bonferroni procedure was employed for multiple testing correction. Whenever there was no significance after P-value adjusting, we simply reported the raw P-values. Similarly, for DE analysis for disease data shown in Fig. 4F, we compared the fold changes of ME/CFS genes with those of all genes.

Network analysis

We downloaded the human protein-protein interactions (PPIs) from STRING[30] v12.0, comprising 19,622 proteins and 6,857,702 interactions. High-confidence PPIs (combined score >700) were extracted for downstream analysis, including 16,185 proteins and 236,000 interactions. To mitigate bias from hub proteins[81], we applied the random walk with restart (RWR) algorithm with a restart probability of 0.5. This produced a smoothed network after retaining the top 5% predicted edges (N = 6,243,766). Next, we utilized the Louvain method[82] to decompose the network into different modules. Following algorithm convergence, we obtained 1,261 modules with an average size of 13 nodes.

The enrichment of genes of interest within each module was tested using one-sided Fisher's exact test. Modules with adjusted $P < 0.05$ based on Benjamini-Hochberg (BH) correction were considered significant.

Gene ontology analysis

Gene ontology (GO) analysis was performed using Enrichr[83] and clusterProfiler[36].

Gene expression enrichment analysis

Single cell RNA sequencing (scRNA-seq) of PBMCs from 30 ME/CFS patients and 30 healthy controls was performed as described in Vu et al.[33] and Iu et al.[34] Dimensional plots and marker plots of scRNA-seq were generated with Seurat v4.4.0. We obtained pseudobulk count data for this dataset from the authors for all samples and cell clusters generated in those publications. This included the initial clustering of all PBMCs into 29 clusters[33] as well as 21 clusters from a high resolution re-clustering of T lymphoid cells[34]. Gene set enrichment analysis (GSEA) was performed comparing ME/CFS and controls within each gene cluster for custom gene lists including the 115 genes and the four significant modules from the network analysis (M9, M15, M18, M20). The input ranking is the Log2FC from DESeq2 analysis of the pseudobulk count data. The genes included in the GSEA ranked list for each cluster are in the top quartile based on mean normalized counts from DESeq2. GSEA was performed with the fgsea R package[84] with the following parameters: eps = 0, minSize = 5, maxSize = 1000, nPermSimple = 10000. P values are determined by comparing each gene list to many permutations of random gene lists of the same size, followed by the Benjamini and Hochberg FDR correction procedure ($q < 0.05$).

Proteomics enrichment analysis

Previously published[31], fully normalized proteomics data was downloaded from mapmecfs.org. 4,790 unique human proteins were detected with the SomaScan aptamer-based assay in the plasma of 20 ME/CFS and 20 control subjects (all females). The 4,790 proteins included 57 of the 115 genes of interest identified here. GSEA was performed with the same gene lists and methods as above for the single-cell RNAseq data.The median Log2 fold change ME/CFS versus control was used as the input ranking for GSEA. For proteins with multiple measurements from different aptamers, the one with the highest |Log2FC| was used to prevent duplicates.

MAGMA analysis

Gene-level analyses of GWAS data were conducted using MAGMA v1.10[85]. GWAS variants were mapped to genes using an annotation window of 10kb both upstream and downstream of

the gene body. Linkage disequilibrium (LD) was adjusted based on the 1KG EUR panel. The Mean model (snp-wise=mean) was applied to derive the gene-level *P*-values.

Genetic correlation analysis

For rare variant association study and GWAS data, we compared the *P*-values of ME/CFS genes with those of all background genes using a one-sided Wilcoxon rank-sum test. The Bonferroni procedure was adopted for *P*-value adjusting when available; otherwise the raw *P*-values were reported. For Mendelian disorder gene sets, we used a one-sided Fisher's exact test to evaluate the enrichment of ME/CFS genes within each disease gene set, followed by the Bonferroni correction.

References

1. Lim, E.-J. *et al.* Systematic review and meta-analysis of the prevalence of chronic fatigue syndrome/myalgic encephalomyelitis (CFS/ME). *J Transl Med* **18**, 100 (2020).
2. Institute of Medicine, Board on the Health of Select Populations & Committee on the Diagnostic Criteria for Myalgic Encephalomyelitis/Chronic Fatigue Syndrome. *Beyond Myalgic Encephalomyelitis/Chronic Fatigue Syndrome: Redefining an Illness*. (National Academies Press, 2015).
3. Baxter, H., Speight, N. & Weir, W. Life-Threatening Malnutrition in Very Severe ME/CFS. *Healthcare* **9**, 459 (2021).
4. Maksoud, R., Magawa, C., Eaton-Fitch, N., Thapaliya, K. & Marshall-Gradisnik, S. Biomarkers for myalgic encephalomyelitis/chronic fatigue syndrome (ME/CFS): a systematic review. *BMC Med* **21**, 189 (2023).
5. Valdez, A. R. *et al.* Estimating Prevalence, Demographics, and Costs of ME/CFS Using Large Scale Medical Claims Data and Machine Learning. *Front Pediatr* **6**, 412 (2018).
6. Hanson, M. R. The viral origin of myalgic encephalomyelitis/chronic fatigue syndrome. *PLoS Pathog* **19**, e1011523 (2023).
7. Dibble, J. J., McGrath, S. J. & Ponting, C. P. Genetic risk factors of ME/CFS: a critical review. *Hum Mol Genet* **29**, R117–R124 (2020).
8. Hajdarevic, R. *et al.* Genetic association study in myalgic encephalomyelitis/chronic fatigue syndrome (ME/CFS) identifies several potential risk loci. *Brain Behav Immun* **102**, 362–369 (2022).
9. Schlauch, K. A. *et al.* Genome-wide association analysis identifies genetic variations in subjects with myalgic encephalomyelitis/chronic fatigue syndrome. *Transl Psychiatry* **6**, e730 (2016).
10. Claussnitzer, M. *et al.* A brief history of human disease genetics. *Nature* **577**, 179–189 (2020).
11. Bergström, A. *et al.* Insights into human genetic variation and population history from 929 diverse genomes. *Science* **367**, (2020).
12. Li, J. *et al.* Decoding the Genomics of Abdominal Aortic Aneurysm. *Cell* **174**, 1361–1372.e10 (2018).
13. Fiziev, P. P. *et al.* Rare penetrant mutations confer severe risk of common diseases. *Science* **380**, eabo1131 (2023).
14. Halford, J. L. *et al.* Endophenotype effect sizes support variant pathogenicity in monogenic

disease susceptibility genes. *Nat Commun* **13**, 5106 (2022).
15. Huang, Y.-F., Gulko, B. & Siepel, A. Fast, scalable prediction of deleterious noncoding variants from functional and population genomic data. *Nat Genet* **49**, 618–624 (2017).
16. Sundaram, L. *et al.* Predicting the clinical impact of human mutation with deep neural networks. *Nat Genet* **50**, 1161–1170 (2018).
17. Storey, J. D. & Tibshirani, R. Statistical significance for genomewide studies. *Proceedings of the National Academy of Sciences* **100**, 9440–9445 (2003).
18. Wang, K., Li, M. & Hakonarson, H. ANNOVAR: functional annotation of genetic variants from high-throughput sequencing data. *Nucleic Acids Res* **38**, e164 (2010).
19. Petrovski, S., Wang, Q., Heinzen, E. L., Allen, A. S. & Goldstein, D. B. Genic intolerance to functional variation and the interpretation of personal genomes. *PLoS Genet* **9**, e1003709 (2013).
20. Lek, M. *et al.* Analysis of protein-coding genetic variation in 60,706 humans. *Nature* **536**, 285–291 (2016).
21. Karczewski, K. J. *et al.* The mutational constraint spectrum quantified from variation in 141,456 humans. *Nature* **581**, 434–443 (2020).
22. Uhlén, M. *et al.* Proteomics. Tissue-based map of the human proteome. *Science* **347**, 1260419 (2015).
23. Jiang, L. *et al.* A Quantitative Proteome Map of the Human Body. *Cell* **183**, 269–283.e19 (2020).
24. Marshall-Gradisnik, S. & Eaton-Fitch, N. Understanding myalgic encephalomyelitis. *Science* **377**, 1150–1151 (2022).
25. Komaroff, A. L. & Lipkin, W. I. Insights from myalgic encephalomyelitis/chronic fatigue syndrome may help unravel the pathogenesis of postacute COVID-19 syndrome. *Trends Mol Med* **27**, 895–906 (2021).
26. Zhang, S. *et al.* Genome-wide identification of the genetic basis of amyotrophic lateral sclerosis. *Neuron* **110**, 992–1008.e11 (2022).
27. Zhang, S. *et al.* Multiomic analysis reveals cell-type-specific molecular determinants of COVID-19 severity. *Cell Syst* **13**, 598–614.e6 (2022).
28. Zhang, S. *et al.* Deconvolution of polygenic risk score in single cells unravels cellular and molecular heterogeneity of complex human diseases. *bioRxiv* (2024) doi:10.1101/2024.05.14.594252.
29. Zhang, S. *et al.* Deep learning modeling of rare noncoding genetic variants in human motor neurons defines as a therapeutic target for ALS. *medRxiv* (2024) doi:10.1101/2024.03.30.24305115.
30. Szklarczyk, D. *et al.* The STRING database in 2023: protein-protein association networks and functional enrichment analyses for any sequenced genome of interest. *Nucleic Acids Res* **51**, D638–D646 (2023).
31. Germain, A., Levine, S. M. & Hanson, M. R. In-Depth Analysis of the Plasma Proteome in ME/CFS Exposes Disrupted Ephrin-Eph and Immune System Signaling. *Proteomes* **9**, (2021).
32. Comella, P. H. *et al.* A Molecular network approach reveals shared cellular and molecular signatures between chronic fatigue syndrome and other fatiguing illnesses. *medRxiv* (2021) doi:10.1101/2021.01.29.21250755.

33. Vu, L. T. *et al.* Single-cell transcriptomics of the immune system in ME/CFS at baseline and following symptom provocation. *Cell Rep Med* **5**, 101373 (2024).
34. Iu, D. S. *et al.* Transcriptional reprogramming primes CD8+ T cells toward exhaustion in Myalgic encephalomyelitis/chronic fatigue syndrome. *Proc Natl Acad Sci U S A* **121**, e2415119121 (2024).
35. Hashimoto, K. *et al.* Single-cell transcriptomics reveals expansion of cytotoxic CD4 T cells in supercentenarians. *Proc Natl Acad Sci U S A* **116**, 24242–24251 (2019).
36. Yu, G., Wang, L.-G., Han, Y. & He, Q.-Y. clusterProfiler: an R package for comparing biological themes among gene clusters. *OMICS* **16**, 284–287 (2012).
37. Karczewski, K. J. *et al.* Systematic single-variant and gene-based association testing of thousands of phenotypes in 394,841 UK Biobank exomes. *Cell Genom* **2**, 100168 (2022).
38. Lammi, V. *et al.* Genome-wide association study of long COVID. *medRxiv* (2023) doi:10.1101/2023.06.29.23292056.
39. Unger, E. R. *et al.* Myalgic Encephalomyelitis/Chronic Fatigue Syndrome After SARS-CoV-2 Infection. *JAMA Netw Open* **7**, e2423555 (2024).
40. Komaroff, A. L. & Lipkin, W. I. ME/CFS and Long COVID share similar symptoms and biological abnormalities: road map to the literature. *Front Med (Lausanne)* **10**, 1187163 (2023).
41. Zhang, M. J. *et al.* Polygenic enrichment distinguishes disease associations of individual cells in single-cell RNA-seq data. *Nat Genet* **54**, 1572–1580 (2022).
42. COVID-19 Host Genetics Initiative. Mapping the human genetic architecture of COVID-19. *Nature* **600**, 472–477 (2021).
43. Li, X., Ding, H., Feng, G. & Huang, Y. Role of angiotensin converting enzyme in pathogenesis associated with immunity in cardiovascular diseases. *Life Sci.* **352**, 122903 (2024).
44. Mitchell, P. D., Buckley, C., Subramaniam, A., Crowther, S. & Donnelly, S. C. Elevated serum ACE levels in patients with post-acute COVID-19 syndrome. *QJM* **115**, 651–652 (2022).
45. Cutrell, S. *et al.* ACE-inhibitors in hypertension: A historical perspective and current insights. *Curr. Hypertens. Rep.* **25**, 243–250 (2023).
46. Zhang, Y. *et al.* Nicotinamide Phosphoribosyltransferase-elevated NAD+ biosynthesis prevents muscle disuse atrophy by reversing mitochondrial dysfunction. *J. Cachexia Sarcopenia Muscle* **14**, 1003–1018 (2023).
47. Dehhaghi, M. *et al.* The role of kynurenine pathway and NAD+ metabolism in myalgic encephalomyelitis/chronic fatigue syndrome. *Aging Dis.* **13**, 698–711 (2022).
48. Low, R. N., Low, R. J. & Akrami, A. A review of cytokine-based pathophysiology of Long COVID symptoms. *Front. Med. (Lausanne)* **10**, 1011936 (2023).
49. Wang, C.-Y. *et al.* PSMB5 plays a dual role in cancer development and immunosuppression. *Am. J. Cancer Res.* **7**, 2103–2120 (2017).
50. Verbrugge, S. E., Scheper, R. J., Lems, W. F., de Gruijl, T. D. & Jansen, G. Proteasome inhibitors as experimental therapeutics of autoimmune diseases. *Arthritis Res. Ther.* **17**, 17 (2015).
51. Mátyási, B. *et al.* The function of NM23-H1/NME1 and its homologs in major processes linked to metastasis. *Pathol. Oncol. Res.* **26**, 49–61 (2020).

52. Sadeghi Shaker, M., Rokni, M., Mahmoudi, M. & Farhadi, E. Ras family signaling pathway in immunopathogenesis of inflammatory rheumatic diseases. *Front. Immunol.* **14**, 1151246 (2023).
53. Llamosas, N. *et al.* SYNGAP1 controls the maturation of dendrites, synaptic function, and network activity in developing human neurons. *J. Neurosci.* **40**, 7980–7994 (2020).
54. Jeyabalan, N. & Clement, J. P. SYNGAP1: Mind the gap. *Front. Cell. Neurosci.* **10**, 32 (2016).
55. Falls, D. L. Neuregulins: functions, forms, and signaling strategies. *Exp Cell Res* **284**, 14–30 (2003).
56. Griesius, S. *et al.* Reduced expression of the psychiatric risk gene DLG2 (PSD93) impairs hippocampal synaptic integration and plasticity. *Neuropsychopharmacology* **47**, 1367–1378 (2022).
57. Watson, L. M. *et al.* Dominant Mutations in GRM1 Cause Spinocerebellar Ataxia Type 44. *Am J Hum Genet* **101**, 451–458 (2017).
58. Rasmussen, A. H., Rasmussen, H. B. & Silahtaroglu, A. The DLGAP family: neuronal expression, function and role in brain disorders. *Mol Brain* **10**, 43 (2017).
59. Luo, J., Norris, R. H., Gordon, S. L. & Nithianantharajah, J. Neurodevelopmental synaptopathies: Insights from behaviour in rodent models of synapse gene mutations. *Prog Neuropsychopharmacol Biol Psychiatry* **84**, 424–439 (2018).
60. Li, Q. S. *et al.* Genome-wide association study meta-analysis of suicide death and suicidal behavior. *Mol Psychiatry* **28**, 891–900 (2023).
61. Tristán-Clavijo, E. *et al.* A truncating mutation in Alzheimer's disease inactivates neuroligin-1 synaptic function. *Neurobiol Aging* **36**, 3171–3175 (2015).
62. Bakken, I. J. *et al.* Two age peaks in the incidence of chronic fatigue syndrome/myalgic encephalomyelitis: a population-based registry study from Norway 2008-2012. *BMC Med* **12**, 167 (2014).
63. Arron, H. E. *et al.* Myalgic Encephalomyelitis/Chronic Fatigue Syndrome: the biology of a neglected disease. *Front. Immunol.* **15**, 1386607 (2024).
64. Chaudhary, N. S. *et al.* Multi-ancestry GWAS of Long COVID identifies immune-related loci and etiological links to chronic fatigue syndrome, fibromyalgia and depression. *medRxiv* (2024) doi:10.1101/2024.10.07.24315052.
65. Li, H., Zeng, J., Snyder, M. P. & Zhang, S. Modeling gene interactions in polygenic prediction via geometric deep learning. *Genome Res* (2024) doi:10.1101/gr.279694.124.
66. Gaulton, K. J., Preissl, S. & Ren, B. Interpreting non-coding disease-associated human variants using single-cell epigenomics. *Nat Rev Genet* **24**, 516–534 (2023).
67. IGVF Consortium. Deciphering the impact of genomic variation on function. *Nature* **633**, 47–57 (2024).
68. All of Us Research Program Genomics Investigators. Genomic data in the All of Us Research Program. *Nature* **627**, 340–346 (2024).
69. Bateman, L. *et al.* Myalgic Encephalomyelitis/Chronic Fatigue Syndrome: Essentials of Diagnosis and Management. *Mayo Clin Proc* **96**, 2861–2878 (2021).
70. Carruthers, B. M. *et al.* Myalgic encephalomyelitis: International Consensus Criteria. *J Intern Med* **270**, 327–338 (2011).
71. Committee on the Diagnostic Criteria for Myalgic Encephalomyelitis/ChronicFatigue

Syndrome, Board on the Health of Select Populations & Institute of Medicine. *Beyond Myalgic Encephalomyelitis/Chronic Fatigue Syndrome: Redefining an Illness*. (National Academies Press (US), Washington (DC), 2015).
72. Zhou, W. *et al.* Longitudinal multi-omics of host-microbe dynamics in prediabetes. *Nature* **569**, 663–671 (2019).
73. Chen, R. *et al.* Personal omics profiling reveals dynamic molecular and medical phenotypes. *Cell* **148**, 1293–1307 (2012).
74. Lacerda, E. M. *et al.* The UK ME/CFS Biobank for biomedical research on Myalgic Encephalomyelitis/Chronic Fatigue Syndrome (ME/CFS) and Multiple Sclerosis. *Open J Bioresour* **4**, (2017).
75. Moore, G. E. *et al.* Recovery from Exercise in Persons with Myalgic Encephalomyelitis/Chronic Fatigue Syndrome (ME/CFS). *Medicina (Kaunas, Lithuania)* **59**, (2023).
76. Xu, K., Hu, W., Leskovec, J. & Jegelka, S. How Powerful are Graph Neural Networks? *arXiv [cs.LG]* (2018) doi:10.48550/ARXIV.1810.00826.
77. Purcell, S. *et al.* PLINK: a tool set for whole-genome association and population-based linkage analyses. *Am J Hum Genet* **81**, 559–575 (2007).
78. Alexander, D. H., Novembre, J. & Lange, K. Fast model-based estimation of ancestry in unrelated individuals. *Genome Res* **19**, 1655–1664 (2009).
79. 1000 Genomes Project Consortium *et al.* A global reference for human genetic variation. *Nature* **526**, 68–74 (2015).
80. Liu, X., Li, C., Mou, C., Dong, Y. & Tu, Y. dbNSFP v4: a comprehensive database of transcript-specific functional predictions and annotations for human nonsynonymous and splice-site SNVs. *Genome Med* **12**, 103 (2020).
81. Krishnan, A. *et al.* Genome-wide prediction and functional characterization of the genetic basis of autism spectrum disorder. *Nat Neurosci* **19**, 1454–1462 (2016).
82. Blondel, V. D., Guillaume, J.-L., Lambiotte, R. & Lefebvre, E. Fast unfolding of communities in large networks. *arXiv [physics.soc-ph]* (2008) doi:10.48550/ARXIV.0803.0476.
83. Kuleshov, M. V. *et al.* Enrichr: a comprehensive gene set enrichment analysis web server 2016 update. *Nucleic Acids Res* **44**, W90–7 (2016).
84. Korotkevich, G. *et al.* Fast gene set enrichment analysis. *bioRxiv* (2016) doi:10.1101/060012.
85. de Leeuw, C. A., Mooij, J. M., Heskes, T. & Posthuma, D. MAGMA: generalized gene-set analysis of GWAS data. *PLoS Comput. Biol.* **11**, e1004219 (2015).

Figure 1

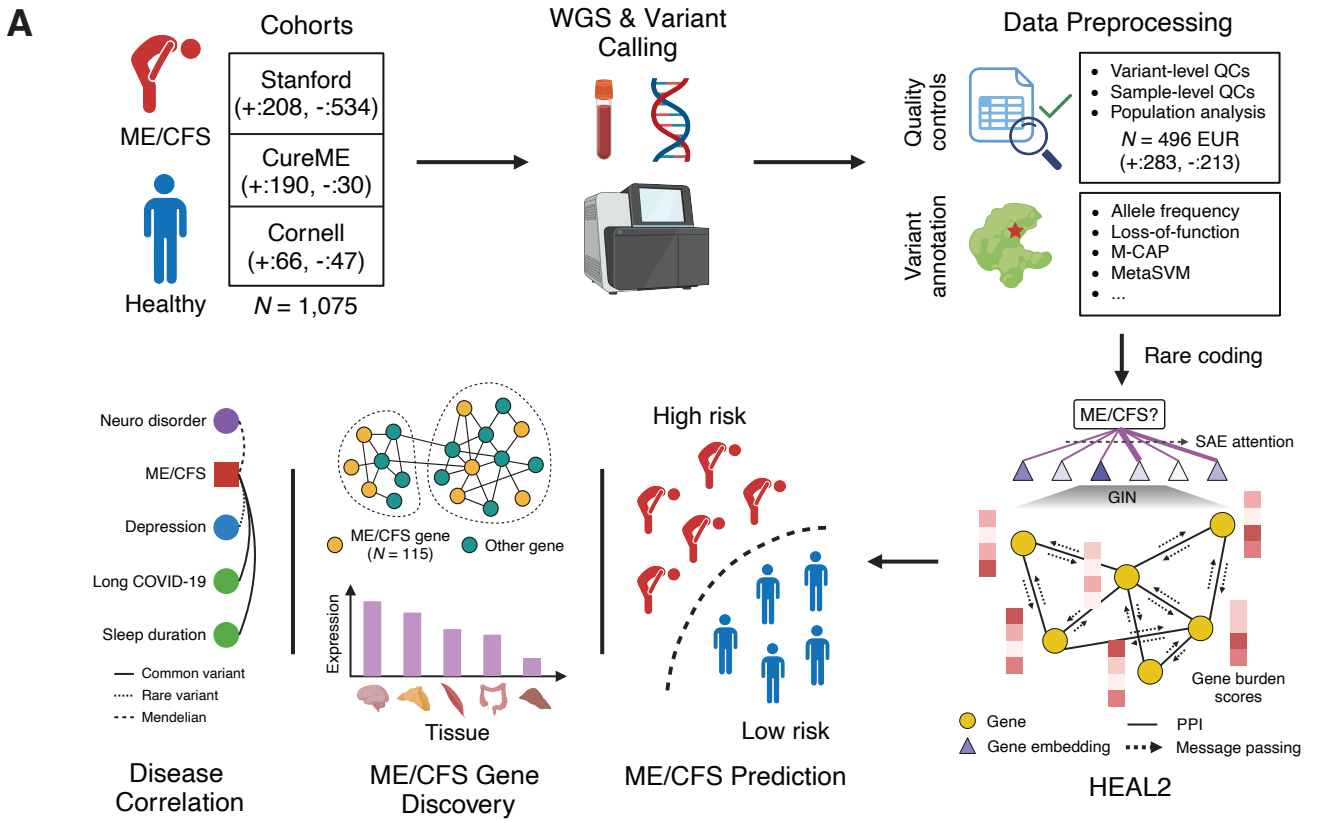
A
Cohorts
ME/CFS
Healthy
Stanford (+:208, -:534)
CureME (+:190, -:30)
Cornell (+:66, -:47)
N = 1,075
WGS & Variant Calling
Data Preprocessing
Quality controls
Variant-level QCs
Sample-level QCs
Population analysis
N = 496 EUR (+:283, -:213)
Variant annotation
Allele frequency
Loss-of-function
M-CAP
MetaSVM
...
Rare coding
ME/CFS?
SAE attention
GIN
Gene burden scores
Gene
Gene embedding
PPI
Message passing
HEAL2
High risk
Low risk
ME/CFS Prediction
ME/CFS gene (N = 115)
Other gene
Expression
Tissue
ME/CFS Gene Discovery
Neuro disorder
ME/CFS
Depression
Long COVID-19
Sleep duration
Common variant
Rare variant
Mendelian
Disease Correlation

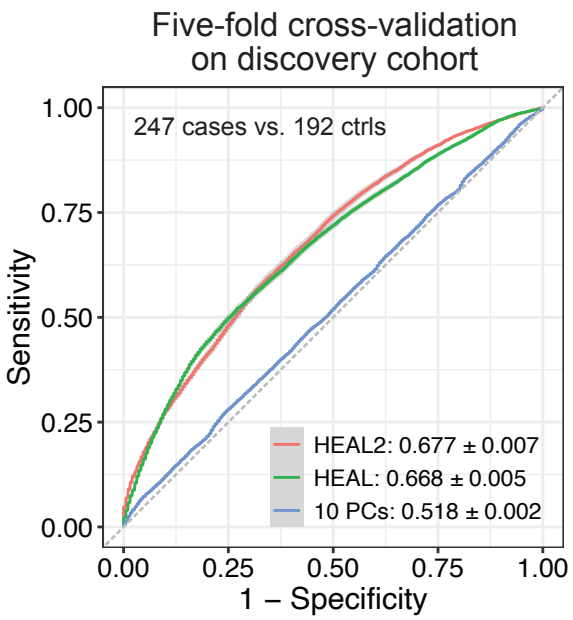
B
Five-fold cross-validation on discovery cohort
247 cases vs. 192 ctrls
Sensitivity
1 – Specificity
HEAL2: 0.677 ± 0.007
HEAL: 0.668 ± 0.005
10 PCs: 0.518 ± 0.002

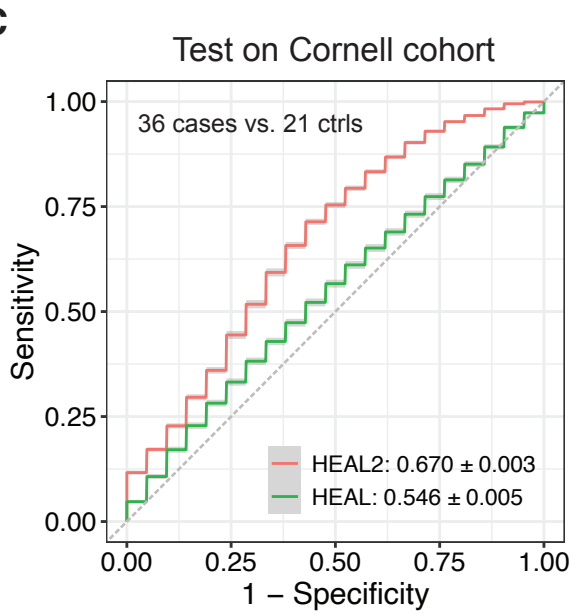
C
Test on Cornell cohort
36 cases vs. 21 ctrls
Sensitivity
1 – Specificity
HEAL2: 0.670 ± 0.003
HEAL: 0.546 ± 0.005

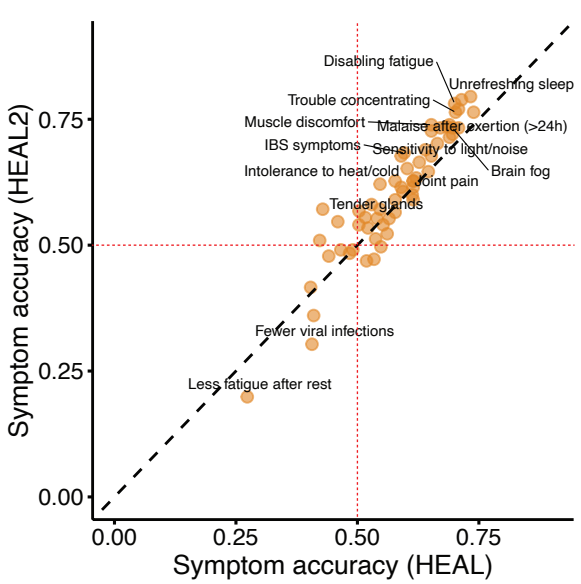
D
Disabling fatigue
Unrefreshing sleep
Trouble concentrating
Muscle discomfort
Malaise after exertion (>24h)
IBS symptoms
Sensitivity to light/noise
Intolerance to heat/cold
Brain fog
Joint pain
Tender glands
Fewer viral infections
Less fatigue after rest
Symptom accuracy (HEAL2)
Symptom accuracy (HEAL)

Figure 2

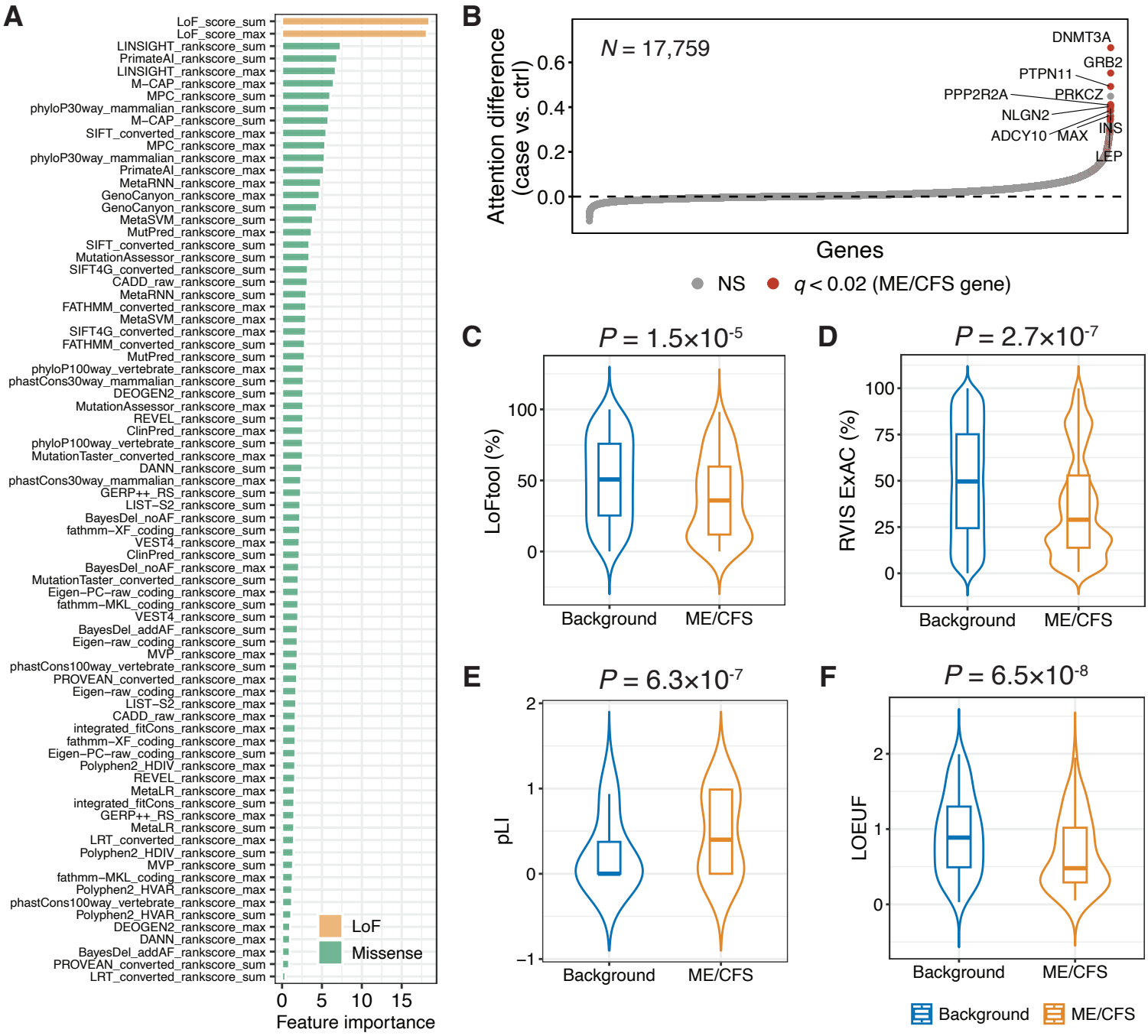
A
LoF_score_sum
LoF_score_max
LINSIGHT_rankscore_sum
PrimateAI_rankscore_sum
LINSIGHT_rankscore_max
M−CAP_rankscore_max
MPC_rankscore_sum
phyloP30way_mammalian_rankscore_sum
M−CAP_rankscore_sum
SIFT_converted_rankscore_max
MPC_rankscore_max
phyloP30way_mammalian_rankscore_max
PrimateAI_rankscore_max
MetaRNN_rankscore_max
GenoCanyon_rankscore_max
GenoCanyon_rankscore_sum
MetaSVM_rankscore_sum
MutPred_rankscore_max
SIFT_converted_rankscore_sum
MutationAssessor_rankscore_sum
SIFT4G_converted_rankscore_sum
CADD_raw_rankscore_sum
MetaRNN_rankscore_sum
FATHMM_converted_rankscore_max
MetaSVM_rankscore_max
SIFT4G_converted_rankscore_max
FATHMM_converted_rankscore_sum
MutPred_rankscore_sum
phyloP100way_vertebrate_rankscore_max
phastCons30way_mammalian_rankscore_sum
DEOGEN2_rankscore_sum
MutationAssessor_rankscore_max
REVEL_rankscore_sum
ClinPred_rankscore_max
phyloP100way_vertebrate_rankscore_sum
MutationTaster_converted_rankscore_max
DANN_rankscore_sum
phastCons30way_mammalian_rankscore_max
GERP++_RS_rankscore_sum
LIST−S2_rankscore_sum
BayesDel_noAF_rankscore_sum
fathmm−XF_coding_rankscore_sum
VEST4_rankscore_max
ClinPred_rankscore_sum
BayesDel_noAF_rankscore_max
MutationTaster_converted_rankscore_sum
Eigen−PC−raw_coding_rankscore_max
fathmm−MKL_coding_rankscore_sum
VEST4_rankscore_sum
BayesDel_addAF_rankscore_sum
Eigen−raw_coding_rankscore_sum
MVP_rankscore_max
phastCons100way_vertebrate_rankscore_sum
PROVEAN_converted_rankscore_max
Eigen−raw_coding_rankscore_max
LIST−S2_rankscore_max
CADD_raw_rankscore_max
integrated_fitCons_rankscore_max
fathmm−XF_coding_rankscore_max
Eigen−PC−raw_coding_rankscore_sum
Polyphen2_HDIV_rankscore_max
REVEL_rankscore_max
MetaLR_rankscore_max
integrated_fitCons_rankscore_sum
GERP++_RS_rankscore_max
MetaLR_rankscore_sum
LRT_converted_rankscore_max
Polyphen2_HDIV_rankscore_sum
MVP_rankscore_sum
fathmm−MKL_coding_rankscore_max
Polyphen2_HVAR_rankscore_max
phastCons100way_vertebrate_rankscore_max
Polyphen2_HVAR_rankscore_sum
DEOGEN2_rankscore_max
DANN_rankscore_max
BayesDel_addAF_rankscore_max
PROVEAN_converted_rankscore_sum
LRT_converted_rankscore_sum
LoF
Missense
0 5 10 15
Feature importance
B
N = 17,759
Attention difference (case vs. ctrl)
0.0 0.2 0.4 0.6
DNMT3A
GRB2
PTPN11
PPP2R2A
PRKCZ
NLGN2
ADCY10
MAX
INS
LEP
Genes
NS
q < 0.02 (ME/CFS gene)
C
P = 1.5×10-5
LoFtool (%)
0 50 100
Background
ME/CFS
D
P = 2.7×10-7
RVIS ExAC (%)
0 25 50 75 100
Background
ME/CFS
E
P = 6.3×10-7
pLI
−1 0 1 2
Background
ME/CFS
F
P = 6.5×10-8
LOEUF
0 1 2
Background
ME/CFS
Background
ME/CFS

Figure 3

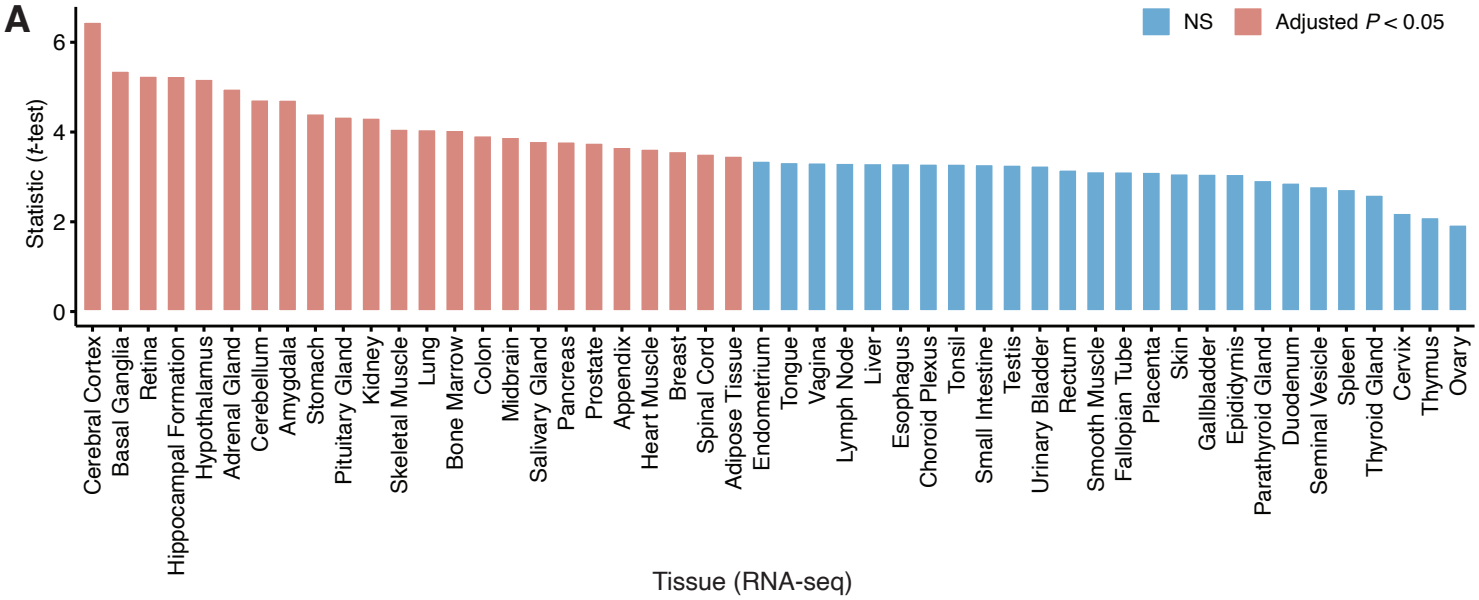
A
NS
Adjusted P < 0.05
Statistic (t-test)
0
2
4
6
Cerebral Cortex
Basal Ganglia
Retina
Hippocampal Formation
Hypothalamus
Adrenal Gland
Cerebellum
Amygdala
Stomach
Pituitary Gland
Kidney
Skeletal Muscle
Lung
Bone Marrow
Colon
Midbrain
Salivary Gland
Pancreas
Prostate
Appendix
Heart Muscle
Breast
Spinal Cord
Adipose Tissue
Endometrium
Tongue
Vagina
Lymph Node
Liver
Esophagus
Choroid Plexus
Tonsil
Small Intestine
Testis
Urinary Bladder
Rectum
Smooth Muscle
Fallopian Tube
Placenta
Skin
Gallbladder
Epididymis
Parathyroid Gland
Duodenum
Seminal Vesicle
Spleen
Thyroid Gland
Cervix
Thymus
Ovary
Tissue (RNA-seq)

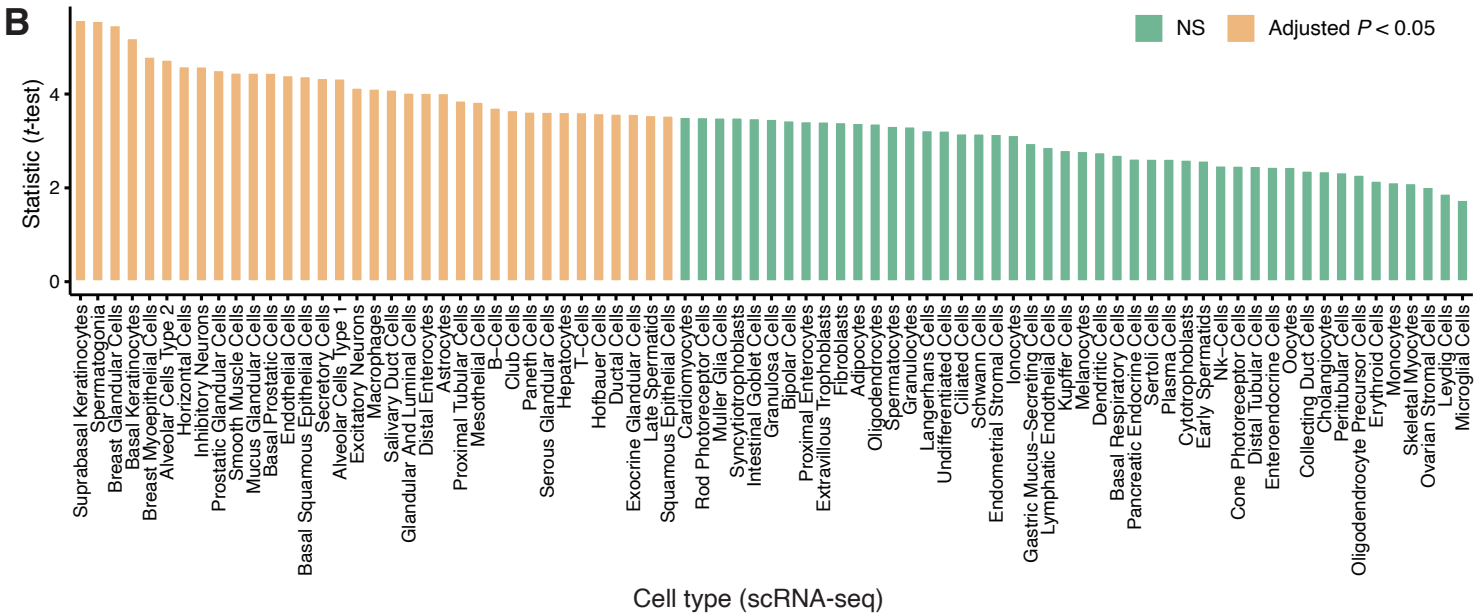
B
NS
Adjusted P < 0.05
Statistic (t-test)
0
2
4
Suprabasal Keratinocytes
Spermatogonia
Breast Glandular Cells
Basal Keratinocytes
Breast Myoepithelial Cells
Alveolar Cells Type 2
Horizontal Cells
Inhibitory Neurons
Prostatic Glandular Cells
Smooth Muscle Cells
Mucus Glandular Cells
Basal Prostatic Cells
Endothelial Cells
Basal Squamous Epithelial Cells
Secretory Cells
Alveolar Cells Type 1
Excitatory Neurons
Macrophages
Salivary Duct Cells
Glandular And Luminal Cells
Distal Enterocytes
Astrocytes
Proximal Tubular Cells
Mesothelial Cells
B–Cells
Club Cells
Paneth Cells
Serous Glandular Cells
Hepatocytes
T–Cells
Hofbauer Cells
Ductal Cells
Exocrine Glandular Cells
Late Spermatids
Squamous Epithelial Cells
Cardiomyocytes
Rod Photoreceptor Cells
Muller Glia Cells
Syncytiotrophoblasts
Intestinal Goblet Cells
Granulosa Cells
Bipolar Cells
Proximal Enterocytes
Extravillous Trophoblasts
Fibroblasts
Adipocytes
Oligodendrocytes
Spermatocytes
Granulocytes
Langerhans Cells
Undifferentiated Cells
Ciliated Cells
Schwann Cells
Endometrial Stromal Cells
Ionocytes
Gastric Mucus–Secreting Cells
Lymphatic Endothelial Cells
Kupffer Cells
Melanocytes
Dendritic Cells
Basal Respiratory Cells
Pancreatic Endocrine Cells
Sertoli Cells
Plasma Cells
Cytotrophoblasts
Early Spermatids
Nk–Cells
Cone Photoreceptor Cells
Distal Tubular Cells
Enteroendocrine Cells
Oocytes
Collecting Duct Cells
Cholangiocytes
Peritubular Cells
Oligodendrocyte Precursor Cells
Erythroid Cells
Monocytes
Skeletal Myocytes
Ovarian Stromal Cells
Leydig Cells
Microglial Cells
Cell type (scRNA-seq)

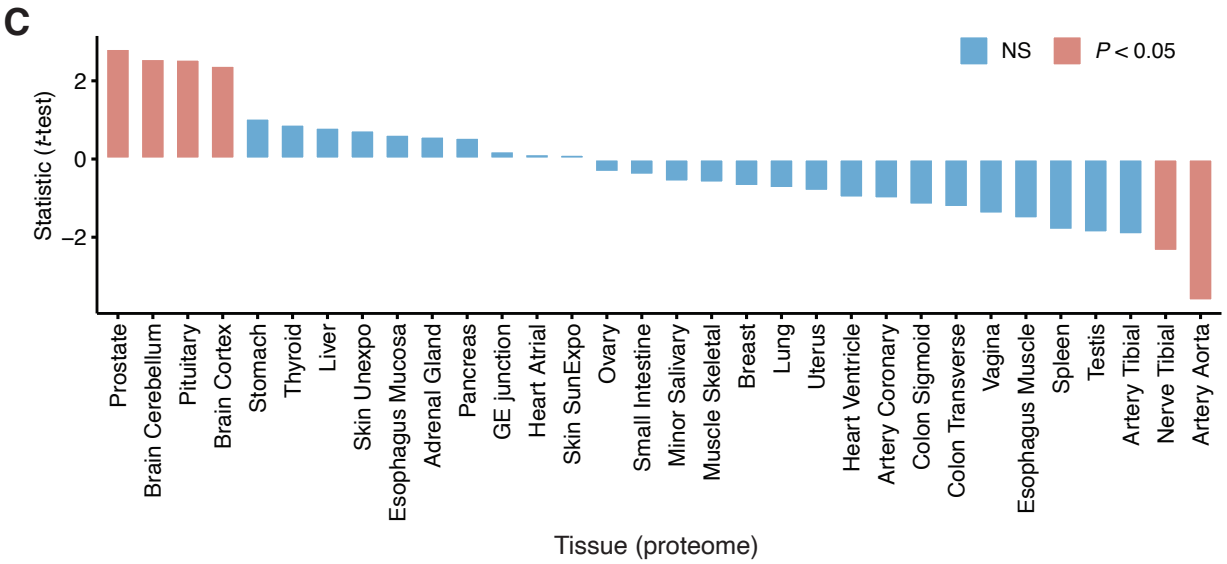
C
NS
P < 0.05
Statistic (t-test)
−2
0
2
Prostate
Brain Cerebellum
Pituitary
Brain Cortex
Stomach
Thyroid
Liver
Skin Unexpo
Esophagus Mucosa
Adrenal Gland
Pancreas
GE junction
Heart Atrial
Skin SunExpo
Ovary
Small Intestine
Minor Salivary
Muscle Skeletal
Breast
Lung
Uterus
Heart Ventricle
Artery Coronary
Colon Sigmoid
Colon Transverse
Vagina
Esophagus Muscle
Spleen
Testis
Artery Tibial
Nerve Tibial
Artery Aorta
Tissue (proteome)

Figure 4

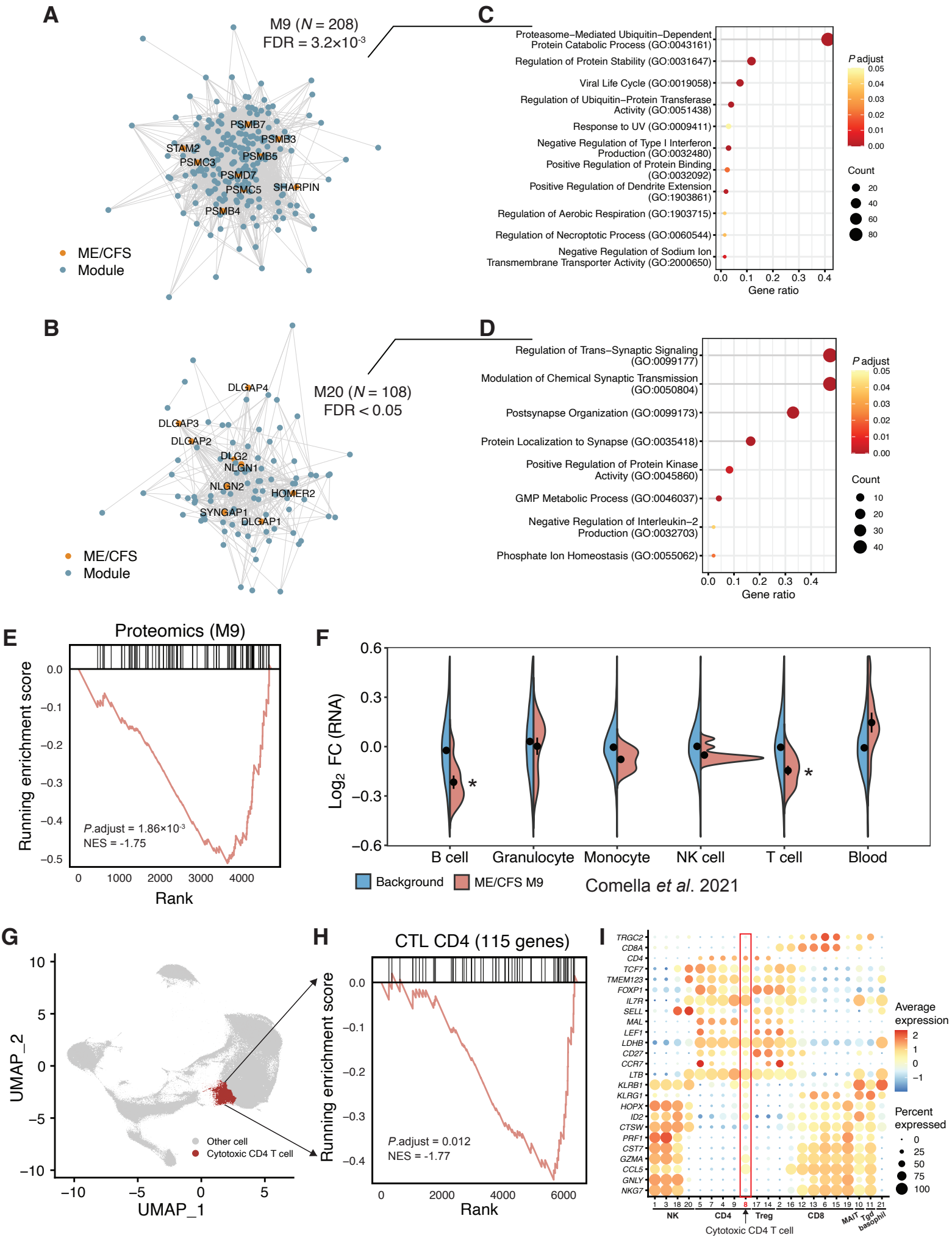
A
M9 (N = 208)
FDR = 3.2×10-3
PSMB7
PSMB3
STAM2
PSMB5
PSMC3
PSMD7
PSMC5
SHARPIN
PSMB4
ME/CFS
Module
C
Proteasome-Mediated Ubiquitin-Dependent Protein Catabolic Process (GO:0043161)
Regulation of Protein Stability (GO:0031647)
Viral Life Cycle (GO:0019058)
Regulation of Ubiquitin-Protein Transferase Activity (GO:0051438)
Response to UV (GO:0009411)
Negative Regulation of Type I Interferon Production (GO:0032480)
Positive Regulation of Protein Binding (GO:0032092)
Positive Regulation of Dendrite Extension (GO:1903861)
Regulation of Aerobic Respiration (GO:1903715)
Regulation of Necroptotic Process (GO:0060544)
Negative Regulation of Sodium Ion Transmembrane Transporter Activity (GO:2000650)
Gene ratio
P adjust
Count
B
M20 (N = 108)
FDR < 0.05
DLGAP4
DLGAP3
DLGAP2
DLG2
NLGN1
NLGN2
HOMER2
SYNGAP1
DLGAP1
ME/CFS
Module
D
Regulation of Trans-Synaptic Signaling (GO:0099177)
Modulation of Chemical Synaptic Transmission (GO:0050804)
Postsynapse Organization (GO:0099173)
Protein Localization to Synapse (GO:0035418)
Positive Regulation of Protein Kinase Activity (GO:0045860)
GMP Metabolic Process (GO:0046037)
Negative Regulation of Interleukin-2 Production (GO:0032703)
Phosphate Ion Homeostasis (GO:0055062)
Gene ratio
P adjust
Count
E
Proteomics (M9)
Running enrichment score
P.adjust = 1.86×10-3
NES = -1.75
Rank
F
Log2 FC (RNA)
B cell
Granulocyte
Monocyte
NK cell
T cell
Blood
Background
ME/CFS M9
Comella et al. 2021
G
UMAP_2
UMAP_1
Other cell
Cytotoxic CD4 T cell
H
CTL CD4 (115 genes)
Running enrichment score
P.adjust = 0.012
NES = -1.77
Rank
I
TRGC2
CD8A
CD4
TCF7
TMEM123
FOXP1
IL7R
SELL
MAL
LEF1
LDHB
CD27
CCR7
LTB
KLRB1
KLRG1
HOPX
ID2
CTSW
PRF1
CST7
GZMA
CCL5
GNLY
NKG7
NK
CD4
Treg
CD8
MAIT
Tgd
basophil
Cytotoxic CD4 T cell
Average expression
Percent expressed

Figure 5

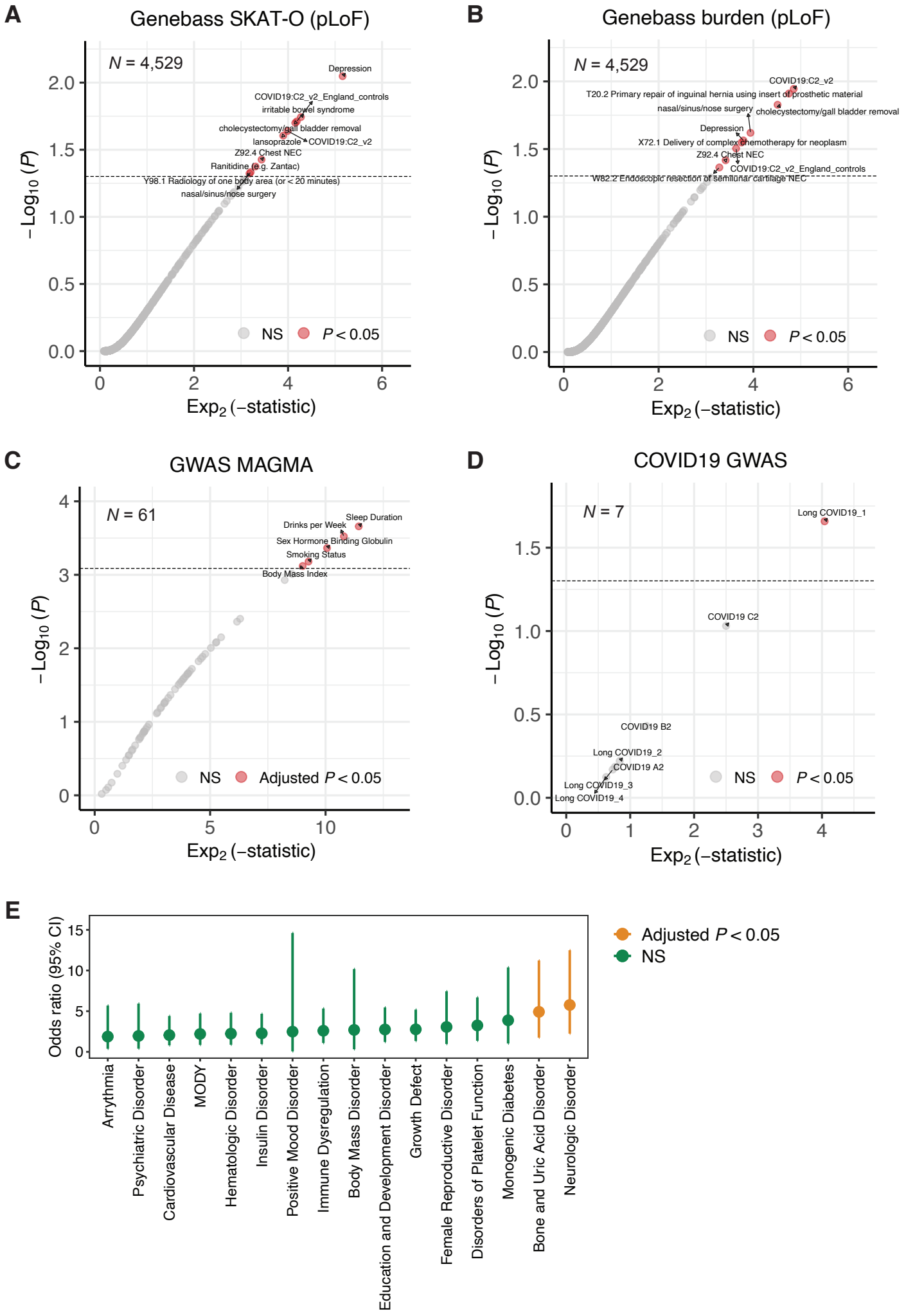
A
Genebass SKAT-O (pLoF)
N = 4,529
Depression
COVID19:C2_v2_England_controls
irritable bowel syndrome
cholecystectomy/gall bladder removal
lansoprazole
COVID19:C2_v2
Z92.4 Chest NEC
Ranitidine (e.g. Zantac)
Y98.1 Radiology of one body area (or < 20 minutes)
nasal/sinus/nose surgery
NS
P < 0.05
−Log10 (P)
Exp2 (−statistic)
B
Genebass burden (pLoF)
N = 4,529
COVID19:C2_v2
T20.2 Primary repair of inguinal hernia using insert of prosthetic material
nasal/sinus/nose surgery
cholecystectomy/gall bladder removal
Depression
X72.1 Delivery of complex chemotherapy for neoplasm
Z92.4 Chest NEC
COVID19:C2_v2_England_controls
W82.2 Endoscopic resection of semilunar cartilage NEC
NS
P < 0.05
−Log10 (P)
Exp2 (−statistic)
C
GWAS MAGMA
N = 61
Sleep Duration
Drinks per Week
Sex Hormone Binding Globulin
Smoking Status
Body Mass Index
NS
Adjusted P < 0.05
−Log10 (P)
Exp2 (−statistic)
D
COVID19 GWAS
N = 7
Long COVID19_1
COVID19 C2
COVID19 B2
Long COVID19_2
COVID19 A2
Long COVID19_3
Long COVID19_4
NS
P < 0.05
−Log10 (P)
Exp2 (−statistic)
E
Odds ratio (95% CI)
Adjusted P < 0.05
NS
Arrythmia
Psychiatric Disorder
Cardiovascular Disease
MODY
Hematologic Disorder
Insulin Disorder
Positive Mood Disorder
Immune Dysregulation
Body Mass Disorder
Education and Development Disorder
Growth Defect
Female Reproductive Disorder
Disorders of Platelet Function
Monogenic Diabetes
Bone and Uric Acid Disorder
Neurologic Disorder